MAX-PLANCK-INSTITUT FÜR PLASMAPHYSIK

GARCHING BEI MÜNCHEN

The Influence of Magnetic Fluctuations on Collisional Drift-Wave Turbulence

Suzana J. Camargo, Bruce D. Scott
and Dieter Biskamp

IPP 6/336 December 1995

Die nachstehende Arbeit wurde im Rahmen des Vertrages zwischen dem Max-Planck-Institut für Plasmaphysik und der Europäischen Atomgemeinschaft über die Zusammenarbeit auf dem Gebiete der Plasmaphysik durchgeführt.

Abstract

A two-dimensional collisional drift-wave turbulence model, which includes magnetic fluctuations is studied using numerical simulations. This model has as limits the electrostatic Hasegawa-Wakatani equations and the two-dimensional magnetohydrodynamic equations. The main parameter of the system $\beta = 4\pi n_0 T/B_0^2$ determines the strength of the magnetic fluctuations. For $\beta = 0.001$ the system is electrostatic, while for $\beta = 10$ it is electromagnetic. The properties of the turbulence were analyzed by increasing the value of β and comparing with the characteristics of the Hasegawa-Wakatani system. The linear analysis shows that differences enter only for $\beta = 10$, and that the adiabatic regime is most sensitive to variation of β. The saturated state of the turbulence for different cases was studied using many different diagnostics. The transfer of free energy and other nonlinear invariants were directly computed. The principal effect of the magnetic fluctuations is to diminish the adiabaticity of the system by reducing the immediacy of the dissipative coupling between the density and electrostatic potential fluctuations, since this coupling must go through the magnetic fluctuations. The computed particle transport decreases strongly for higher values of β.

1 Introduction

The physical processes of plasma transport in magnetic confinement devices, e.g. tokamaks, are not well understood. The transport of particles and energy is anomalous, i.e. the observed values are much larger than what is calculated by considering Coulomb collisions between the particles. It is usually assumed that the anomalous transport is due to the observed turbulent fluctuations of density, electric potential and magnetic field. The presence of spatial plasma gradients in the plasma lead to collective oscillations called drift-waves. The main effect of the drift-wave dynamics in the macroscopic scale is an anomalous diffusion of particles and energy along the corresponding gradient of the plasma density or temperature. Drift-wave turbulence is therefore considered as a possible cause for the anomalous transport in tokamaks [1, 3]. Drift-wave turbulence theories are usually electrostatic, i.e. the fluctuations of the magnetic field are neglected [3]. However, it is not clear whether electrostatic or magnetic fluctuations (or both) are responsible for the anomalous transport [4]. Determining which fluctuation mechanism is dominant in driving the transport would provide a major constraint in the viability of various theories. An experimental determination of which effect is dominant would require a major advance in experiment diagnostics [5].

Experimental measurements of the fluctuation of the magnetic field are difficult. Until recently only measurements of magnetic fluctuations at the plasma edge have been possible [4]. Even at the edge of the tokamak, it is difficult to make quantitative calculations of the effects of the magnetic fluctuations. Besides the coherent and high-beta MHD activity, such as sawteeth, fishbones, tearing modes and ELM's, broadband fluctuations are observed [2]. These incoherent magnetic fluctuations have amplitudes $\delta B_\perp/B \sim 10^{-4} - 10^{-5}$, with $\delta B_\perp \gg \delta B_\parallel$, are fairly isotropic perpendicularly to $\mathbf{B}$ and increase with decreasing minor radius [1, 2, 4]. Magnetic fluctuations have been considered a possible contributor for the transport in various tokamaks [6]. The magnetic fluctuations have been found both to correlate and not correlate with plasma transport in different machines. A correlation between the magnetic fluctuations and the quality of confinement is found during various transitions of confinement regimes (L-mode, H-mode, and ELM's) [2]. The Reversed Field Pinch (RFP) is ideal to study magnetic fluctuations as they are typically two orders of magnitude larger than those observed in tokamaks; theories can then be tested over a wider dynamic range than in tokamaks [6, 7, 8]. Recent experimental results for the RFP show that the magnetic fluctuations and the electrostatic fluctuations are related and conclude that suppressing the tearing mode activity could lead to a reduction of the edge electrostatic fluctuations [9]. By contrast, recent measurements in the tokamak TEXT indicate that the magnetic fluctuations are not responsible for the transport of heat [10]. The fact that the level of magnetic fluctuations in the plasma boundary region is very small can lead to the conclusion that they do not play a significant role for transport [11], even in the case of the RFP [8]. However, the issue cannot be assumed to be clear without a more complete investigation.

Many models have tried to relate the magnetic fluctuations to the transport in the plasma [1, 12, 13, 14]. The theories have very different approaches towards the problem.

Typically these theories utilize quasi-linear approximations and neglect self-consistent field effects. Some models calculate the anomalous electron thermal conduction due to stochastic magnetic field, but without specifying the source of the magnetic fluctuations (see e.g. [15, 16]). Other models consider, for instance, the anomalous electron thermal conductivity due to high-m ballooning modes [17]. Many studies of magnetic turbulence suppose a linear relation among the modes, relying in quasi-linear or weak turbulence approaches or concentrate on the magnetic fluctuations associated with finite sized magnetic islands and microtearing modes [13, 18]. Magnetohydrodynamic (MHD) turbulence [19, 20], which disregards the fluctuations of the density, was also studied thoroughly and has properties similar to fluid turbulence.

Although drift-waves are basically electrostatic modes, they also have a small magnetic component, which can also lead to transport [21]. Magnetic fluctuations at the plasma edge that may be associated with electromagnetic drift-waves have been observed in the TCA tokamak [22]. Quasi-linear studies of electromagnetic drift-waves have been performed by many authors (see [1] and references therein). Calculations for stochastic diffusion of electrons in tokamaks due to a spectrum of electromagnetic drift fluctuations obtained diffusion coefficient scales approximating experimental scalings [3]. Other electromagnetic studies of drift-wave turbulence include the collisionless model of Molvig *et al.* [23] and the numerical simulations of Waltz [24]. A recent numerical study of a similar system with magnetic and density fluctuations, but disregarding potential fluctuations, observes three different turbulent states, even for identical parameters, making the turbulence state nonunique [25]. In [26] the anomalous transport due to electromagnetic drift-Alfvén turbulence was studied using DIA (Direct Interaction Approximation) techniques, concluding that the electromagnetic contribution to transport by circulating electrons is important, while the transport dominated by trapped electrons is not affected by magnetic fluctuations. This result contrasts with another study of drift-Alfvén turbulence [27], which concluded that electrostatic fluctuations alone regulate the transport. Another recent interesting analytical study of drift-wave theories, derived using a Lagrangian method, shows that the magnetic fluctuations may not be negligible even for $\beta \ll 1$ [28].

Three-dimensional numerical simulations of drift-wave turbulence confirm earlier indications that collisional drift-wave turbulence is the fundamental ingredient underlying tokamak edge and scrape-off layer turbulence [29]. It has been also suggested that edge turbulence could originate in the core plasma region [30], where the magnetic fluctuations can be of fundamental importance. Experimental evidence of drift-wave like instabilities in the core region of the tokamak is given in [31]. Recent numerical simulations suggest that the transition from resistive ballooning to drift-wave turbulence as a possible model for the L-H transition [32]. Therefore, it is of fundamental importance to understand the role of the magnetic fluctuations in a simple drift-wave turbulence model, to see better how their effect should be considered in more realistic models.

The aim of this work is then to analyze the effect of the magnetic fluctuations in drift-wave dynamics. The magnetic fluctuations bring different physical effects into the system. We want to determine which are these effects and what is their role into the system. It is also important to understand whether the electrostatic approximation is a valid hypoth-

esis when studying turbulence at the edge of the tokamak. We consider the magnetic fluctuations in a simple model for drift-wave turbulence. The properties of the Hasegawa-Wakatani system have been studied thoroughly in two and three dimensions [33] - [38]. This model is generalized by including the magnetic fluctuations in the equations. We then analyze how these fluctuations modify the properties of the electrostatic model. Related forms of these equations were first derived independently by Hasegawa and Wakatani [39] and Hazeltine [40]. The model chosen has as its extreme limits the two-dimensional (2-D) Hasegawa-Wakatani model [33] and the 2-D MHD model [19, 20], both well known, which makes the interpretation of the results obtained easier. Bekki and Kaneda [41] performed low-resolution numerical simulations of this model in three dimensions analyzing the formation of structures, but did not study the turbulent state. A related electromagnetic drift-wave system was studied numerically by Waltz [24]. A similar study has already been done for a more general set of equations [42], but there numerical restrictions did not allow a thorough study of the electromagnetic effects. The numerical scheme employed here is similar to the one used for the Hasegawa-Wakatani model [34] and in other studies with a sheared magnetic field [43].

The principal result of this study is that the role of the magnetic fluctuations is to reduce the immediacy of the coupling between the density and the electrostatic potential fluctuations in an otherwise electrostatic system. That is, the basic physics is that of drift-waves with a certain enhancement of the nonadiabatic character due to the internal dynamics of the magnetic fluctuations. The transport is always nearly electrostatic. This result shows that the drift-wave part of a more complicated system can never be neglected, as shown previously in the case of rippling modes [44]. Specifically, microtearing [25] is unlikely to have any significant role on its own in anomalous transport in tokamaks.

In Section 2 the model and its main characteristics are described. The linear properties of the system are studied in Section 3. Section 4 describes the main results of the numerical simulations. In section 5, we study the linear mode interaction and the nonlinear transfer of energy, enstrophy and magnetic potential. The conclusions are presented in section 6.

2 Model and invariants

2.1 Electromagnetic drift-wave equations

This model is a generalization of the Hasegawa-Wakatani system in slab geometry when magnetic fluctuations ψ are also considered. The total magnetic field $\mathbf{B}$ has an uniform component in the z direction, B_0, and the magnetic fluctuations are in the plane (x, y),

$$\mathbf{B} = B_0 \hat{e}_z - \nabla \times \psi \hat{e}_z. \tag{1}$$

As usual, the electron density n is given by $n = n_0 (1 + n_1/n_0)$, with $n_1 \ll n_0$. The equilibrium density $n_0(x)$ has a density gradient in the negative x direction, such that the equilibrium density scale $L_n = n_0 / |dn_0/dx|$ is a constant. Additionally, the electrons are

considered isothermal and the ions cold, such that $T_i \ll T_e = T$. Temperature gradients and fluctuations are neglected.

We obtain the equations of the model from the Braginskii two-fluid equations [45]. The drift-wave dispersion scale ρ_s and the sound speed c_s are defined respectively as $\rho_s = c\sqrt{M_i T}/eB$, $c_s = \sqrt{T/M_i}$. The fluctuations are scaled according to $\tilde{\phi} = (e\phi/T)\,(L_n/\rho_s)$, $\tilde{n} = (n_1/n_0)\,(L_n/\rho_s)$, $\tilde{\psi} = (\psi/B_0\rho_s)\,(L_n/\rho_s)$ and the dimensionless variables are defined as $x \to x/\rho_s$, $y \to y/\rho_s$, $z \to z/L_n$, $t \to tc_s/L_n$.

The equations that describe our model are then given by

$$\frac{d_E}{dt}\tilde{\Omega} = \nabla_{\parallel}\tilde{J} - \mu\nabla_{\perp}^4\tilde{\Omega}, \tag{2}$$

$$\frac{d_E}{dt}\tilde{n} = -\frac{\partial\tilde{\phi}}{\partial y} + \nabla_{\parallel}\tilde{J} - \mu\nabla_{\perp}^4\tilde{n}, \tag{3}$$

$$\frac{\partial\tilde{\psi}}{\partial t} = -\frac{\partial\tilde{\psi}}{\partial y} + \nabla_{\parallel}\left(\tilde{n} - \tilde{\phi}\right) - \eta_*\beta\tilde{J} - \mu\nabla_{\perp}^4\tilde{\psi}, \tag{4}$$

where

$$\tilde{\Omega} = \nabla_{\perp}^2\tilde{\phi}, \tag{5}$$

$$\tilde{J} = -\frac{1}{\beta}\nabla_{\perp}^2\tilde{\psi}, \tag{6}$$

$$\frac{d_E}{dt} = \frac{\partial}{\partial t} + \left(\hat{\mathbf{z}} \times \nabla_{\perp}\tilde{\phi}\right)\cdot\nabla_{\perp}, \tag{7}$$

$$\nabla_{\parallel} = iK_{\parallel} - \left(\hat{\mathbf{z}} \times \nabla_{\perp}\tilde{\psi}\right)\cdot\nabla_{\perp}, \tag{8}$$

$$\beta = \frac{4\pi n_0 T}{B_0^2}, \tag{9}$$

$$\eta_* = \frac{\eta_{\parallel}c^2}{4\pi}\frac{L_n}{c_s\rho_s^2}. \tag{10}$$

$\partial/\partial z$ was replaced by the parallel wavenumber $K_{\parallel} = k_z L_n$, which will be taken as a constant. A term of the type $-\mu\nabla_{\perp}^4\tilde{n}$ was added in each equation. These terms are hyper-viscosity like terms and by taking appropriate values of μ confine the dissipation to the smallest scales resolved in the system. An equivalent form of these equations can be found in [41].

From the analysis of the equations, it is expected that the electromagnetic effects will be mainly controlled by β. For $\beta \ll 1$ the current $\tilde{J}$ corresponds to weak magnetic fields $\tilde{\psi}$ (see equation (6)) and the corrections to the parallel operator (equation (8)) and Ohm's law (equation (4) for $\tilde{\psi} \to 0$) are negligible. We are therefore interested in studying the effect of large values of β in the model. Similar versions of this model were first obtained in [39, 40].

The Hasegawa-Wakatani equations are obtained from the electromagnetic drift-wave equations (2) - (4) in the limit $\tilde{\psi} \to 0$ and $\tilde{J} = iK_{\parallel}\left(\tilde{n} - \tilde{\phi}/\left(\eta_*\beta\right)\right)$. The Hasegawa-

Wakatani equations are linearly cross-coupled through the adiabaticity parameter

$$\mathcal{C} = \frac{K_{\|}^2}{\beta \eta_*}. \tag{11}$$

For $\mathcal{C} \gg 1$, there is an adiabatic regime, with the cross-coupling forcing $\tilde{n}$ to mimic $\tilde{\phi}$, which collects at the large scales [34]. On the other hand, for $\mathcal{C} \ll 1$, the hydrodynamic regime, the weakness of the cross-coupling causes $\tilde{n}$ to exhibit pronounced gradient sheets as it is cascaded to small scales, a feature of a passively advected scalar [34]. The 2-D MHD equations [19] are obtained from the electromagnetic drift equations (2)-(4) in the limit of constant density (n = constant) and $K_{\|} = 0$. The electromagnetic drift-wave equations have then as extreme limits two well known systems, the Hasegawa-Wakatani equations (electrostatic limit) [33] and the 2-D MHD equations (electromagnetic limit) [19]. An interesting discussion of the electrostatic and electromagnetic limits can be found in [40].

For the electromagnetic drift-wave equations there are 3 free parameters that determine the turbulent state: $K_{\|}$, β and η. As the behavior for a fixed $\mathcal{C}$ is already known, it is interesting to vary these parameters such that the value of $\mathcal{C}$ is kept constant. The parameter that is of greatest interest is β, as it determines the intensity of the magnetic fluctuations. In order to keep $\mathcal{C}$ constant we also vary η, keeping $K_{\|}$ constant. As we increase β, the value of the resistivity η is then diminished, which helps to intensify the effect of the magnetic fluctuations in the system.

2.2 Invariants of the Model

The invariants of the purely nonlinear subset of the electromagnetic drift-wave equations are the total fluctuation free energy (herein *energy*)

$$E = \frac{1}{2} \int d^2x \left(\left| \nabla_\perp \tilde{\phi} \right|^2 + \tilde{n}^2 + \frac{1}{\beta} \left| \nabla_\perp \tilde{\psi} \right|^2 \right) = E^V + E^N + E^M, \tag{12}$$

the generalized enstrophy

$$U = \frac{1}{2} \int d^2x \left(\tilde{n} - \nabla_\perp^2 \tilde{\phi} \right)^2 = \frac{1}{2} \int d^2x \, (\tilde{n} - \tilde{\Omega})^2, \tag{13}$$

and the magnetic potential

$$A = \frac{1}{2} \int d^2x \, \tilde{\psi}^2. \tag{14}$$

The energy was mentioned as an invariant of this model in [40, 41], but the other two invariants were not considered. The Hasegawa-Wakatani system also has the total energy E (with $E^M = 0$) and the generalized enstrophy U as invariants [33, 34]. On the other hand, the 2-D MHD system has the total energy E (with $E^N = 0$), the magnetic potential A and the cross-helicity H as invariants [19] ($H = \int d^2x \, \mathbf{v} \cdot \mathbf{B} = \int d^2x \, \nabla_\perp \tilde{\phi} \cdot \nabla_\perp \tilde{\psi}$).

According to the electromagnetic drift-wave equations (2), - (4), the invariants E, U and A, evolve with time as

$$\frac{\partial E}{\partial t} = \Gamma_n - \Gamma_r - \mathcal{D}^E, \tag{15}$$

$$\frac{\partial U}{\partial t} = \Gamma_n - \mathcal{D}^U, \tag{16}$$

$$\frac{\partial A}{\partial t} = \Gamma_a - \Gamma_d - \mathcal{D}^A, \tag{17}$$

where

$$\Gamma_n = -\int d^2x\, \tilde{n}\frac{\partial \tilde{\phi}}{\partial y}, \tag{18}$$

$$\Gamma_r = \eta_* \beta \int d^2x\, \tilde{J}^2, \tag{19}$$

$$\Gamma_d = \eta_* \beta \int d^2x\, \tilde{\psi}\tilde{J}, \tag{20}$$

$$\Gamma_a = iK_\parallel \int d^2x\, \tilde{\psi}\left(\tilde{n} - \tilde{\phi}\right), \tag{21}$$

$$\mathcal{D}^E = \mu \int d^2x\, \left(-\tilde{\phi}\nabla_\perp^4\tilde{\Omega} + \tilde{n}\nabla_\perp^4\tilde{n} + \tilde{J}\nabla_\perp^4\tilde{\psi}\right), \tag{22}$$

$$\mathcal{D}^U = \mu \int d^2x\, \left(\tilde{n} - \tilde{\Omega}\right)\nabla_\perp^4\left(\tilde{n} - \tilde{\Omega}\right), \tag{23}$$

$$\mathcal{D}^A = \mu \int d^2x\, \tilde{\psi}\nabla_\perp^4\tilde{\psi}. \tag{24}$$

Γ_n, the source of energy, is the rate at which the energy is extracted from the density gradient. Γ_r is the rate at which the energy is resistively dissipated, and Γ_d the rate that the magnetic potential is resistively dissipated. Γ_a is the source of the magnetic potential, and is proportional to the nonadiabaticity of $\tilde{\phi}$ and $\tilde{n}$ (for $\tilde{n} = \tilde{\phi}$, $\Gamma_a = 0$). The dissipation terms $\mathcal{D}^E$, $\mathcal{D}^U$, and $\mathcal{D}^A$ are due to the introduction of viscous like terms in equations (2)-(4).

3 Linear Analysis

3.1 Linear Growth Rate

The linearized system is first solved analytically, to gain a better understanding of the nonlinear and linear properties. By linearizing and Fourier decomposing equations (2) - (4), assuming a modal dependence of the type $e^{i(\mathbf{k}\cdot\mathbf{x}-\omega t)}$, we obtain

$$\left(\omega + i\mu k^4\right)\tilde{\phi}_\mathbf{k} - \frac{K_\parallel}{\beta}\tilde{\psi}_\mathbf{k} = 0 \tag{25}$$

$$k_y\tilde{\phi}_\mathbf{k} - \left(\omega + i\mu k^4\right)\tilde{n}_\mathbf{k} - \frac{K_\parallel}{\beta}k^2\tilde{\psi}_\mathbf{k} = 0 \tag{26}$$

$$iK_\parallel\tilde{\phi}_\mathbf{k} - iK_\parallel\tilde{n}_\mathbf{k} + \left(-i\left(\omega + i\mu k^4\right) + ik_y + \eta k^2\right)\tilde{\psi}_\mathbf{k} = 0 \tag{27}$$

The dispersion relation obtained from these equations is

$$\left(\omega + i\mu k^4\right)^3 + i\left(\eta k^2 + ik_y\right)\left(\omega + i\mu k^4\right)^2 - \frac{K_\parallel^2}{\beta}(1+k^2)\left(\omega + i\mu k^4\right) + \frac{K_\parallel^2}{\beta}k_y = 0. \quad (28)$$

The solutions of this equation are given by

$$\omega_1 = -\frac{i}{3}\left(\eta k^2 + ik_y + 3\mu k^4\right) - \frac{2^{1/3}\mathcal{A}}{3\mathcal{F}} + \frac{\mathcal{F}}{3\ 2^{1/3}}, \quad (29)$$

$$\omega_2 = -\frac{i}{3}\left(\eta k^2 + ik_y + 3\mu k^4\right) + \frac{\left(1+i\sqrt{3}\right)\mathcal{A}}{3\ 2^{2/3}\mathcal{F}} - \frac{\left(1-i\sqrt{3}\right)\mathcal{F}}{6\ 2^{1/3}}, \quad (30)$$

$$\omega_3 = -\frac{i}{3}\left(\eta k^2 + ik_y + 3\mu k^4\right) + \frac{\left(1-i\sqrt{3}\right)\mathcal{A}}{3\ 2^{2/3}\mathcal{F}} - \frac{\left(1+i\sqrt{3}\right)\mathcal{F}}{6\ 2^{1/3}}, \quad (31)$$

where

$$\mathcal{A} = \left(\eta k^2 + ik_y\right)^2 - 3\frac{K_\parallel^2}{\beta}\left(1+k^2\right), \quad (32)$$

$$\mathcal{B} = -9i\frac{K_\parallel^2}{\beta}\left(1+k^2\right)\left(\eta k^2 + ik_y\right) + 2i\left(\eta k^2 + ik_y\right)^3 - 27\frac{K_\parallel^2}{\beta}k_y, \quad (33)$$

$$\mathcal{F} = \left(\mathcal{B} + \left(4\mathcal{A}^3 + \mathcal{B}^2\right)^{1/2}\right)^{1/3}. \quad (34)$$

The linear growth rate is given by the maximum of the imaginary part of the solutions, that is

$$\gamma(\mathbf{k}) = \max\left(\mathrm{Im}\,\omega_1(\mathbf{k}), \mathrm{Im}\,\omega_2(\mathbf{k}), \mathrm{Im}\,\omega_3(\mathbf{k})\right), \quad (35)$$

and the correspondent real part is $\omega_R(\mathbf{k})$.

In Fig. 1 we show the main properties of the linear growth rate γ and ω_R. The variation of γ and ω_R with different values of β ($\beta = 0.001, 0.1, 1, 5, 10$) and corresponding values of η for $\mathcal{C} = 1$, $K_\parallel = 1$, $k_x = 0$ and $\mu = 0$, is shown in Figs. 1(a) and 1(b). In Fig. 1(c) we show the maximum growth rate $\gamma_{\max}$ as a function of β for $\mathcal{C} = 0.1, 1, 5$ and $k_x = 0$, $K_\parallel = 1$ and $\mu = 0$. The value of $k_{\max}$ (k that corresponds to $\gamma_{\max}$) as a function of β is shown in Fig. 1(d).

By analyzing Fig. 1(a), one can see that for higher β values the linear growth rate is smaller. This property will have an important role in our numerical simulations, as for higher β it takes a longer time for the system to reach a saturated state. This fact is more important in the adiabatic regime ($\mathcal{C} = 5$), which has smaller growth rates, than in the hydrodynamic regime ($\mathcal{C} = 0.1$), as can be seen in Fig. 1(c). When varying β, the linear properties will only have noticeable changes for $\beta \gtrsim 1$ (see Figs. 1(c) and 1(d)).

3.2 Linear phase-shifts

It is interesting to obtain the relations among the different fluctuating fields in the system, linearly and nonlinearly. From the linearized electromagnetic drift-wave equations (25) -

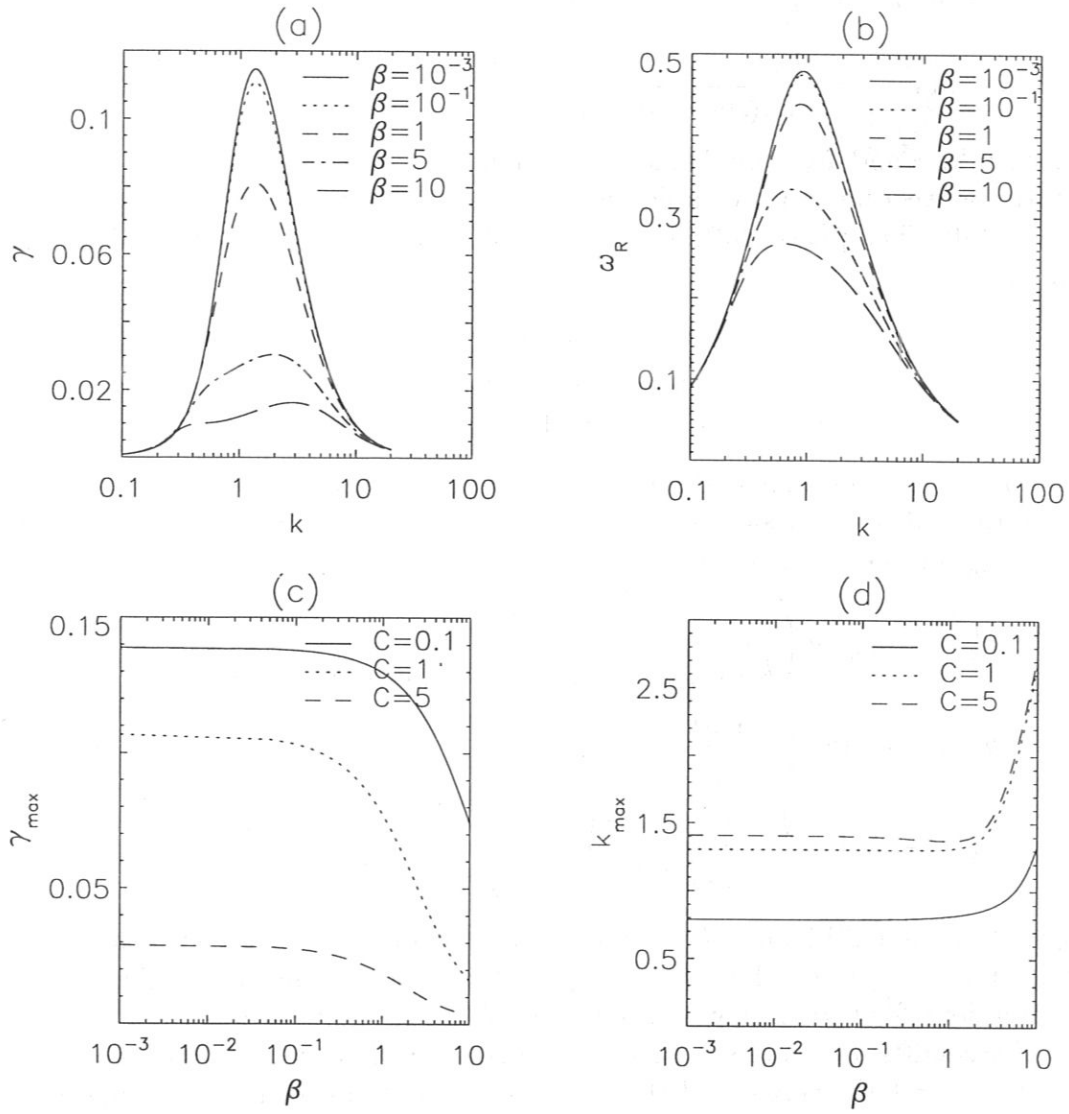

Figure 1: The linear growth rate $\gamma(k)$ (a) and $\omega_R(k)$ (b) for $\mathcal{C} = 1$ and different values of β. The maximum of the linear growth rate $\gamma_{\max}$ (c) and the corresponding wave-number $k_{\max}$ (d) as a function of β for $\mathcal{C} = 0.1, 1, 5$.

(27), expressions for the relations between the fluctuating fields $\widetilde{\phi}_{\mathbf{k}}$, $\widetilde{n}_{\mathbf{k}}$, $\widetilde{\psi}_{\mathbf{k}}$ can be calculated

$$\widetilde{n}_{\mathbf{k}} = f_{\mathbf{k}}\widetilde{\phi}_{\mathbf{k}} = -\frac{\left(k^2\left(\omega_R + i\left(\gamma + \mu k^4\right)\right) - k_y\right)}{\left(\omega_R + i\left(\gamma + \mu k^4\right)\right)}\widetilde{\phi}_{\mathbf{k}} \tag{36}$$

$$\widetilde{\phi}_{\mathbf{k}} = g_{\mathbf{k}}\widetilde{\psi}_{\mathbf{k}} = \frac{\beta}{K_{\parallel}}\left(\omega_R + i\left(\gamma + \mu k^4\right)\right)\widetilde{\psi}_{\mathbf{k}} \tag{37}$$

$$\widetilde{n}_{\mathbf{k}} = h_{\mathbf{k}}\widetilde{\psi}_{\mathbf{k}} = \frac{K_{\parallel}}{\beta}\frac{1}{\left(\omega_R + i\left(\gamma + \mu k^4\right)\right)}\left(\frac{k_y}{\left(\omega_R + i\left(\gamma + \mu k^4\right)\right)} - k^2\right)\widetilde{\psi}_{\mathbf{k}}, \tag{38}$$

where for each $\mathbf{k}$, γ and ω_R were defined in section 3.1.

The ratio between any two complex numbers can be given in terms of an amplitude and a phase-shift. The phase-shifts between the fluctuating fields $\widetilde{n}_{\mathbf{k}}$, $\widetilde{\phi}_{\mathbf{k}}$ and $\widetilde{\psi}_{\mathbf{k}}$ may be expressed as

$$\delta_{\mathbf{k}} = \mathrm{Im}\log\widetilde{n}^*_{\mathbf{k}}\widetilde{\phi}_{\mathbf{k}}, \tag{39}$$

$$\theta_{\mathbf{k}} = \mathrm{Im}\log\widetilde{\phi}^*_{\mathbf{k}}\widetilde{\psi}_{\mathbf{k}}, \tag{40}$$

$$\alpha_{\mathbf{k}} = \mathrm{Im}\log\widetilde{n}^*_{\mathbf{k}}\widetilde{\psi}_{\mathbf{k}}, \tag{41}$$

which will be directly evaluated from our nonlinear numerical simulations. The linear phase-shifts (described by a superscript "L") are obtained as functions of the response functions $f_{\mathbf{k}}$, $g_{\mathbf{k}}$ and $h_{\mathbf{k}}$, such that

$$\delta^L_{\mathbf{k}} = -\arctan\left(\frac{k_y\left(\gamma + \mu k^4\right)}{k^2\left(\omega_R^2 + \left(\gamma + \mu k^4\right)^2\right) - \omega_R k_y}\right), \tag{42}$$

$$\theta^L_{\mathbf{k}} = -\arctan\left(\frac{\gamma + \mu k^4}{\omega_R}\right), \tag{43}$$

$$\alpha^L_{\mathbf{k}} = -\arctan\left(\frac{\left(\gamma + \mu k^4\right)\left(k^2\left(\omega_R^2 + \left(\gamma + \mu k^4\right)^2\right) - 2k_y\omega_R\right)}{k_y\left(\omega_R^2 - \left(\gamma + \mu k^4\right)^2\right) - k^2\omega_R\left(\omega_R^2 + \left(\gamma + \mu k^4\right)^2\right)}\right). \tag{44}$$

In Figs. 2(a) and 2(b) and $\delta^L_{\mathbf{k}}$ is shown for $\mathcal{C} = 0.1$ with $\beta = 0.001$ and $\beta = 10$ respectively. Figs. 2(c) - 2(f) show $\theta^L_{\mathbf{k}}$ and $\alpha^L_{\mathbf{k}}$ for the same parameters. In Fig. 3 we show the same functions for $\mathcal{C} = 5$. For larger values of $\mathcal{C}$, i.e. in the adiabatic limit ($\mathcal{C} = 5$), the linear phase-shifts are more sensitive to changes in β than in the hydrodynamic limit ($\mathcal{C} = 0.1$). For $\mathcal{C} = 1$ the changes of the linear phase-shifts for increasing values of β are already noticeable. In all regimes, the absolute values of the linear phase-shifts diminish as β increase, this effect being particularly strong for $\mathcal{C} = 5$ (see Fig. 3).

4 Numerical Simulation Results

4.1 Numerical Simulation Details

The electromagnetic drift-wave equations (2)-(4) were solved on a square box of size $L^2 = (2\pi/K_0)^2$ with periodic boundary conditions using a deliased pseudo-spectral algorithm.

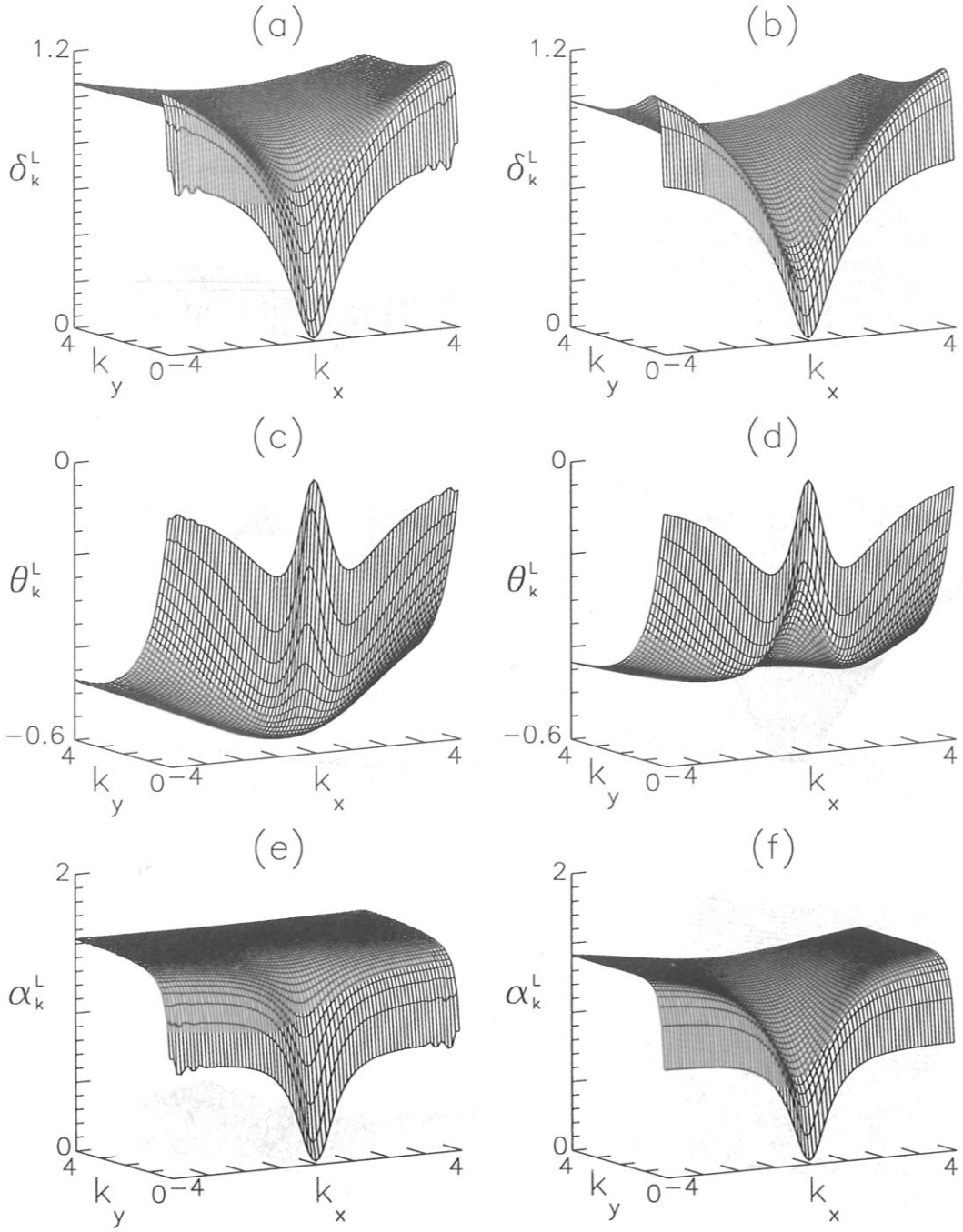

Figure 2: Linear phase-shifts for $\mathcal{C} = 0.1$. $\delta_{\mathbf{k}}^L$ for $\beta = 0.001$ (a) and $\beta = 10$ (b). $\theta_{\mathbf{k}}^L$ for $\beta = 0.001$ (c) and $\beta = 10$ (d). $\alpha_{\mathbf{k}}^L$ for $\beta = 0.001$ (e) and $\beta = 10$ (f)

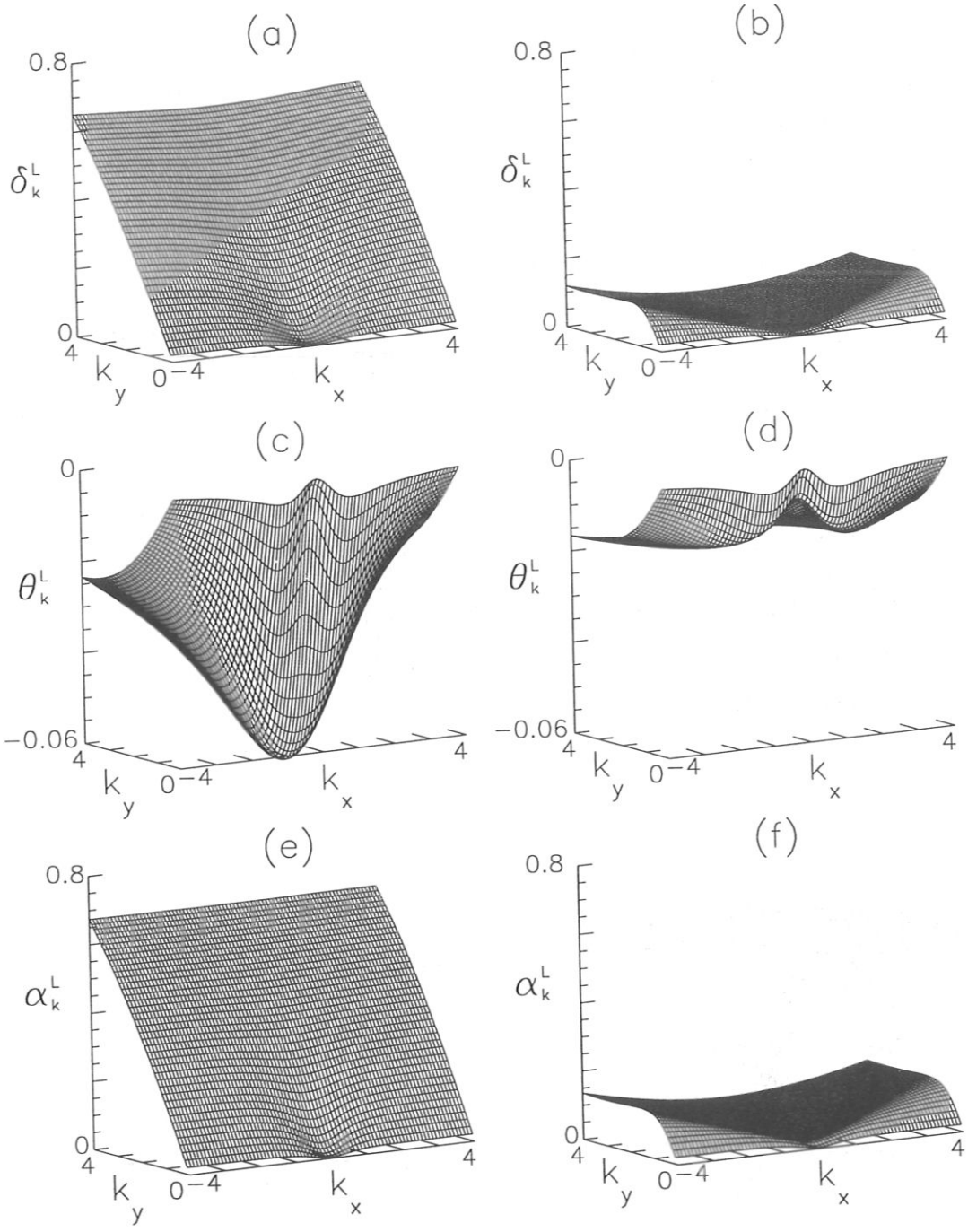

Figure 3: Linear phase-shifts for $\mathcal{C} = 5$. $\delta^L_{\mathbf{k}}$ for $\beta = 0.001$ (a) and $\beta = 10$ (b). $\theta^L_{\mathbf{k}}$ for $\beta = 0.001$ (c) and $\beta = 10$ (d). $\alpha^L_{\mathbf{k}}$ for $\beta = 0.001$ (e) and $\beta = 10$ (f)

The algorithm is very similar to the one employed in studies of the Hasegawa-Wakatani system [34] and for a sheared magnetic field [43]. In most runs, the number of collocation points (grid-size) was 128^2; in some cases a larger number of collocation points (1024^2) was employed. The box size was chosen such that $K_0 = 0.15$. The dissipation parameter μ was taken just large enough to prevent numerical instability, $\mu = 10^{-3}$ in most of the 128^2 runs. Another set of runs was considered to check if any important effects appear when the box is larger. For these runs, we chose $K_0 = 0.0375$, $\mu \sim 10^{-2}$, and in most cases 256^2 collocation points.

Two types of computations were performed: computations for a fixed value of $\mathcal{C}$ (see definition in eq. (11)), with β, η and $K_\parallel$ varying accordingly, and computations with one of the parameters varying (e.g. $K_\parallel$) and the other two parameters fixed (e.g. β and η). The computations with fixed values of $\mathcal{C}$ are the most interesting ones, as the behavior of the system is known at the electrostatic limit (Hasegawa-Wakatani system) and therefore the effects due to the variation of the parameters can be better visualized. The values of $\mathcal{C}$ chosen for our studies, were the same that were already employed for the Hasegawa-Wakatani system: $\mathcal{C} = 0.1, 1, 5$ (see [34]). These values represent three different turbulent regimes in the electrostatic case: a hydrodynamic, an intermediate and an adiabatic regime, respectively. The properties of each of these regimes are described in [34].

The density $\tilde{n}$, potential $\tilde{\phi}$ and magnetic $\tilde{\psi}$ fluctuations were initialized with a random-phase, broad-band field, such that all degrees of freedom are excited with a constant amplitude $\mathcal{M}$

$$\sum_{\mathbf{k}} \tilde{\phi}_{\mathbf{k}} \tilde{\phi}_{\mathbf{k}} = \sum_{\mathbf{k}} \tilde{n}_{\mathbf{k}} \tilde{n}_{\mathbf{k}} = \sum_{\mathbf{k}} \tilde{\psi}_{\mathbf{k}} \tilde{\psi}_{\mathbf{k}} = \mathcal{M}. \tag{45}$$

In most calculations, we chose $\mathcal{M} = 1.e^{-6}$, however in the cases that the linear instability is very weak we considered $\mathcal{M} = 1.e^{-4}$, or even $\mathcal{M} = 1.e-2$; so that the time required for reaching a turbulent saturated state would not be long. The numerical error was tracked in all runs using the energy equation (15); the numerical error was never greater than $0.01E$.

The runs with a finer-grid (1024^2) were obtained by continuing the 128^2 runs and then increasing the number of collocation points to 256^2, 512^2 and finally 1024^2. These runs were performed to obtain better resolution for the spectra and contour plots.

4.2 Properties of the Saturated State

A typical numerical simulation has a linear phase, followed by a saturated turbulent state, which is then maintained long enough for good statistical quantities to be obtained.

In Figs. 4(a) and 4(b), the typical time evolution of the components of the energy E^N, E^V and E^M for a electrostatic case ($\beta = 0.001$) and a electromagnetic case ($\beta = 10$) are shown. By analyzing Fig. 4, one can see that even for the case $\beta = 10$, the magnetic energy E^M is not the dominant component of the total energy E. By increasing β, the role of the kinetic energy E^V diminishes in order to allow E^M to increase (see Table 1). In the hydrodynamic regime, the role of the density is so dominant, that the value of E^N/E is kept constant (0.83), independent of the value of β. By contrast, in the adiabatic regime, the role of each component of the energy is much more affected by the values of β. The

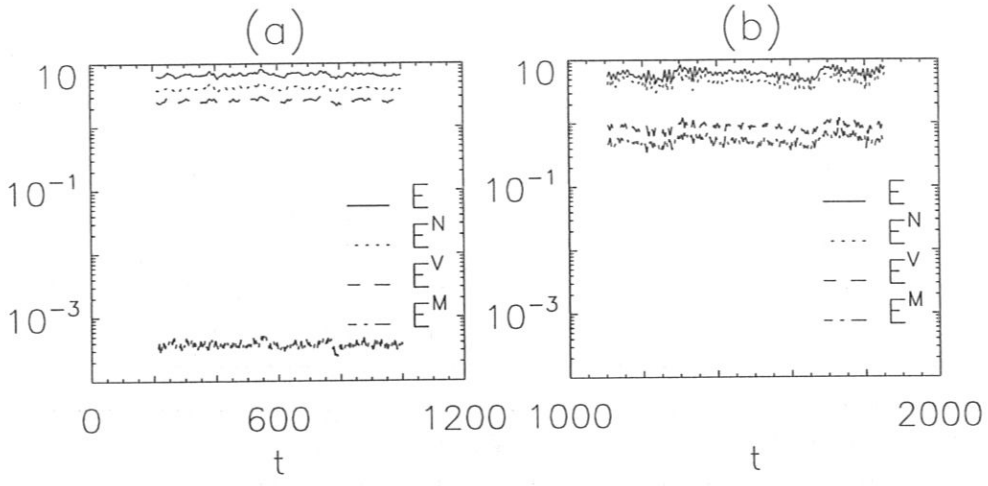

Figure 4: The total energy E and the energy components E^N, E^V, E^M for $\beta = 0.001$ (a) and $\beta = 10$ (b) in the saturated state, with $\mathcal{C} = 1$, $K_\parallel = 1$, and $\mu = 0.001$.

saturation values of the total energy E, the enstrophy U and $\widetilde{\phi}^2/2$ increase as β goes from 0.001 to 0.1 and diminish strongly for $\beta = 10$. The magnetic potential A saturation values increase with β.

The spatial structure of the system is also altered by varying β, which can be seen by analyzing the contour plots. Figs. 5 - 8 show the typical contour plots of $\widetilde{\phi}$, $\widetilde{n}$, $\widetilde{\psi}$, $\widetilde{\Omega}$ and $\widetilde{J}$ in the electrostatic and the electromagnetic regimes for $\mathcal{C} = 0.1$, and $\mathcal{C} = 5$ respectively. For each case, the contour plots were obtained at the same instant of time in a turbulent saturated state. In all contour plots we considered $K_0 = 0.15$, $K_\parallel = 1$, $\mu \sim 10^{-9}$ and 512^2 collocation points. The figures show only the region $[0 : \pi L] \times [0 : \pi L]$, which is one fourth of the real area calculated in the simulations. As usual, $\widetilde{\phi}$ collects at large scales, however by increasing β, $\widetilde{\phi}$ collects at larger scales (Figs. 5 and 7), an effect that is stronger for $\mathcal{C} = 1$ (see also Table 3). In the electromagnetic limit ($\beta = 10$), for $\mathcal{C} = 5$, $\widetilde{n}$ does not mimic $\widetilde{\phi}$, but is more similar to $\widetilde{\psi}$ (Fig. 7). The magnetic fluctuations $\widetilde{\psi}$ have the same behavior in all regimes, always collecting in the larger scales. The vorticity $\widetilde{\Omega}$ usually has fine structures; the presence of large β smooths these structures (Figs. 6 and 8). By contrast, the current $\widetilde{J}$, which collects at average size structures in the electrostatic limit, shows a much finer structure in the electromagnetic limit. This effect, however, appears only in the adiabatic regime, where the electromagnetic effects have a stronger influence on the system.

The angle-averaged spectra of the invariants were also obtained (for the definition see [34]). The spectra exhibit a maximum at a certain wave number k_{SM}. On the high-k side of the maximum k_{SM} there is an inertial range with a decaying power law (e.g. $E_k \sim k^{-a}$) up to the viscous cutoff. The variation of the spectral exponents (e.g. a) with $\mathcal{C}$ and β is shown in Table 2. In the electrostatic limit, the spectral exponents are almost identical

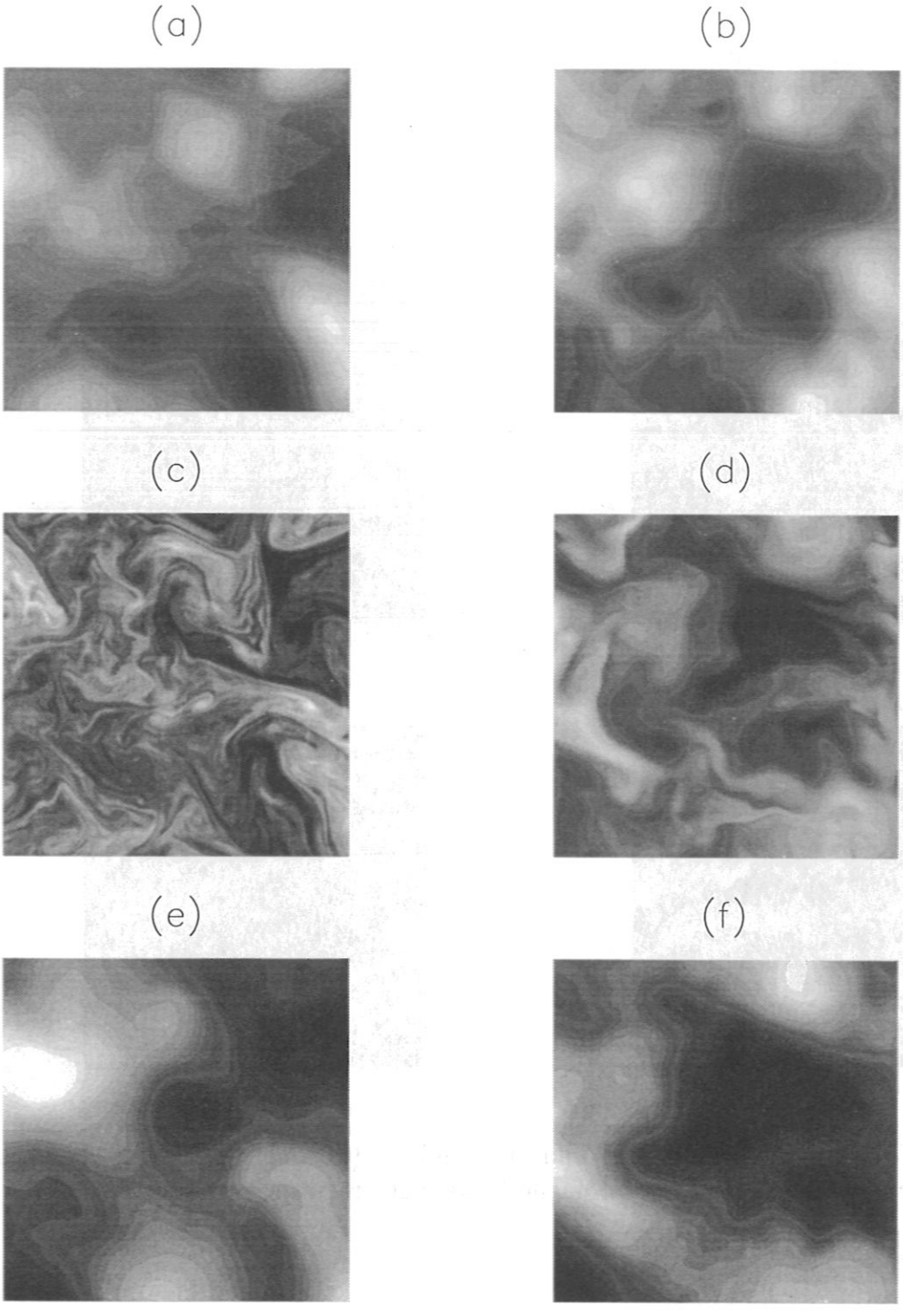

Figure 5: Contour plots of $\widetilde{\phi}$ ((a) and (b)), $\widetilde{n}$ ((c) and (d)) and $\widetilde{\psi}$ ((e) and (f)), for $\mathcal{C} = 0.1$ in the electrostatic ($\beta = 0.001$) and electromagnetic ($\beta = 10$) regimes, respectively.

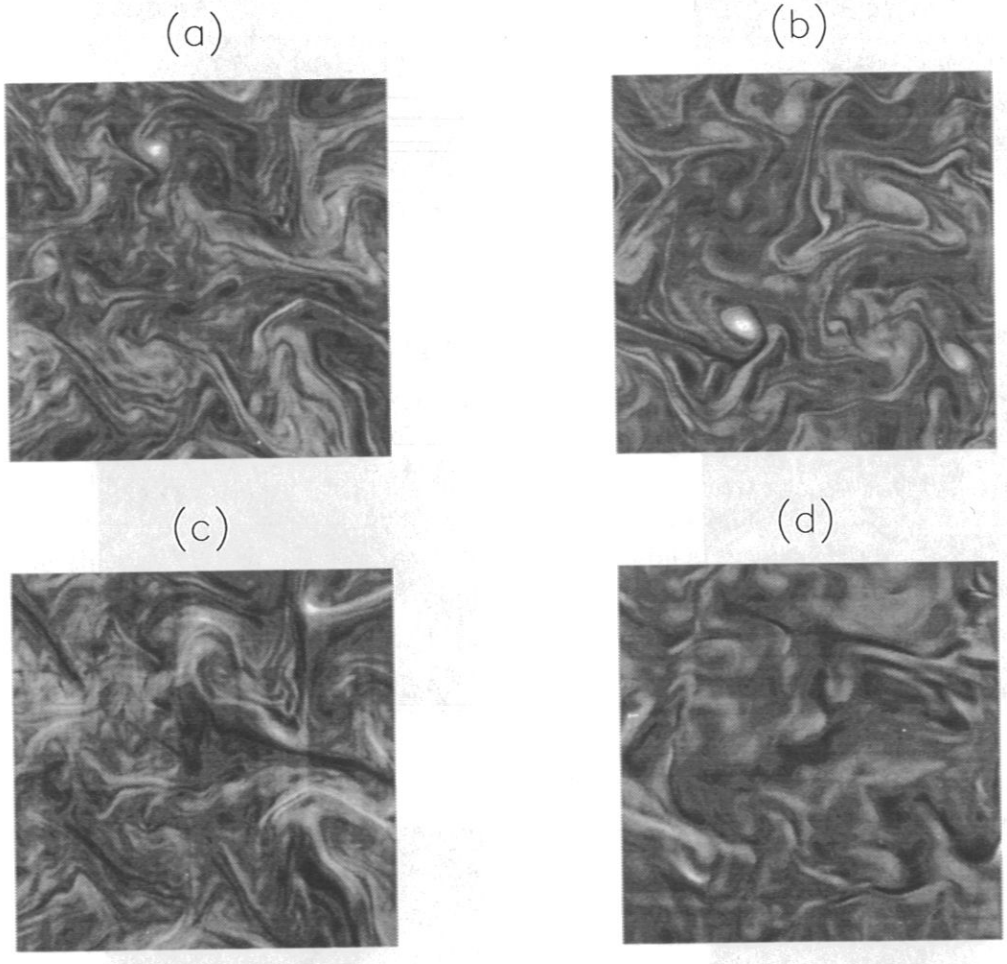

Figure 6: Contour plots of $\tilde{\Omega}$ ((a) and (b)) and $\tilde{J}$ ((c) and (d)), for $\mathcal{C} = 0.1$ in the electrostatic ($\beta = 0.001$) and electromagnetic ($\beta = 10$) regimes, respectively.

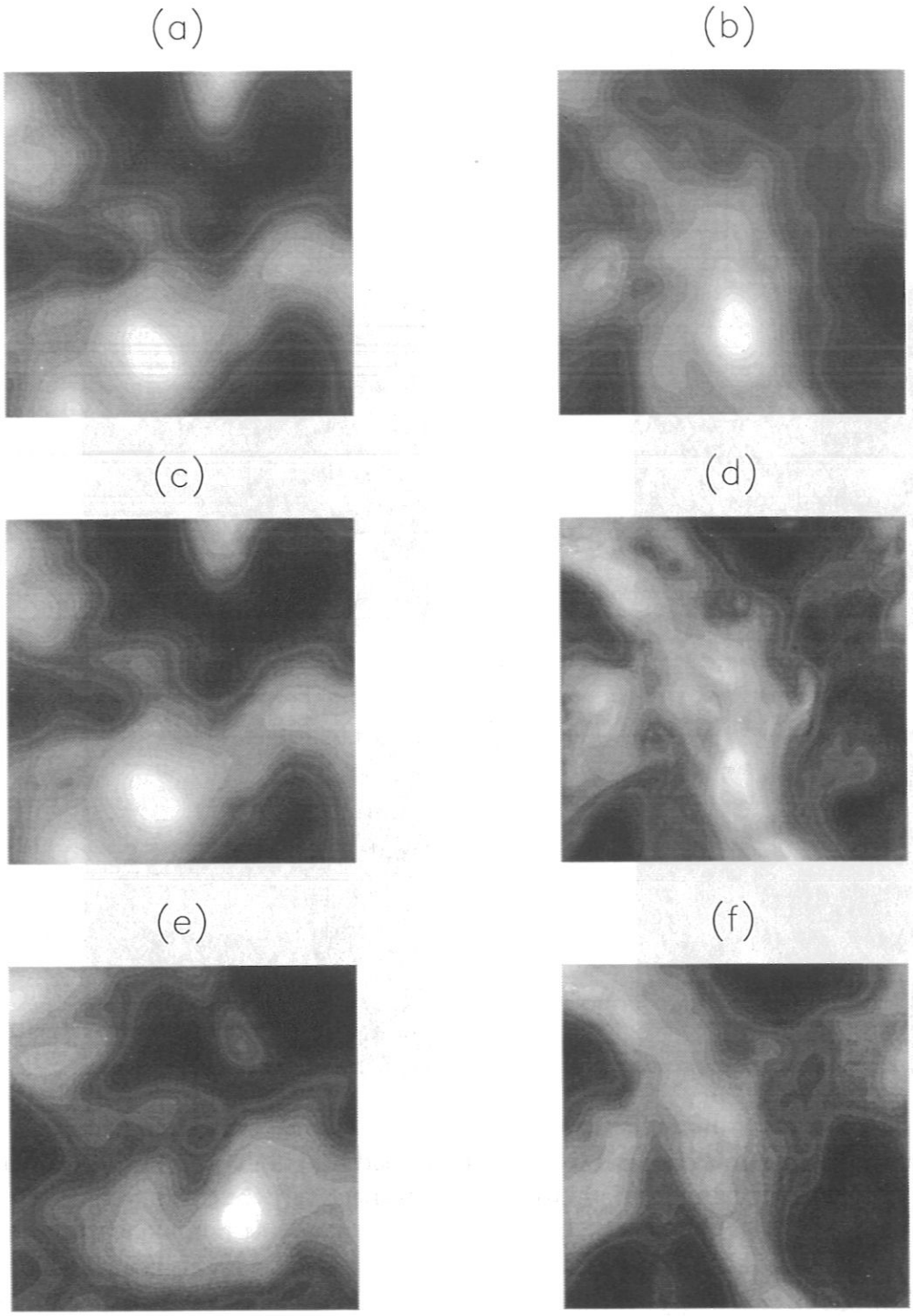

Figure 7: Contour plots of $\widetilde{\phi}$ ((a) and (b)), $\widetilde{n}$ ((c) and (d)) and $\widetilde{\psi}$ ((e) and (f)), for $\mathcal{C} = 5$ in the electrostatic ($\beta = 0.001$) and electromagnetic ($\beta = 10$) regimes, respectively.

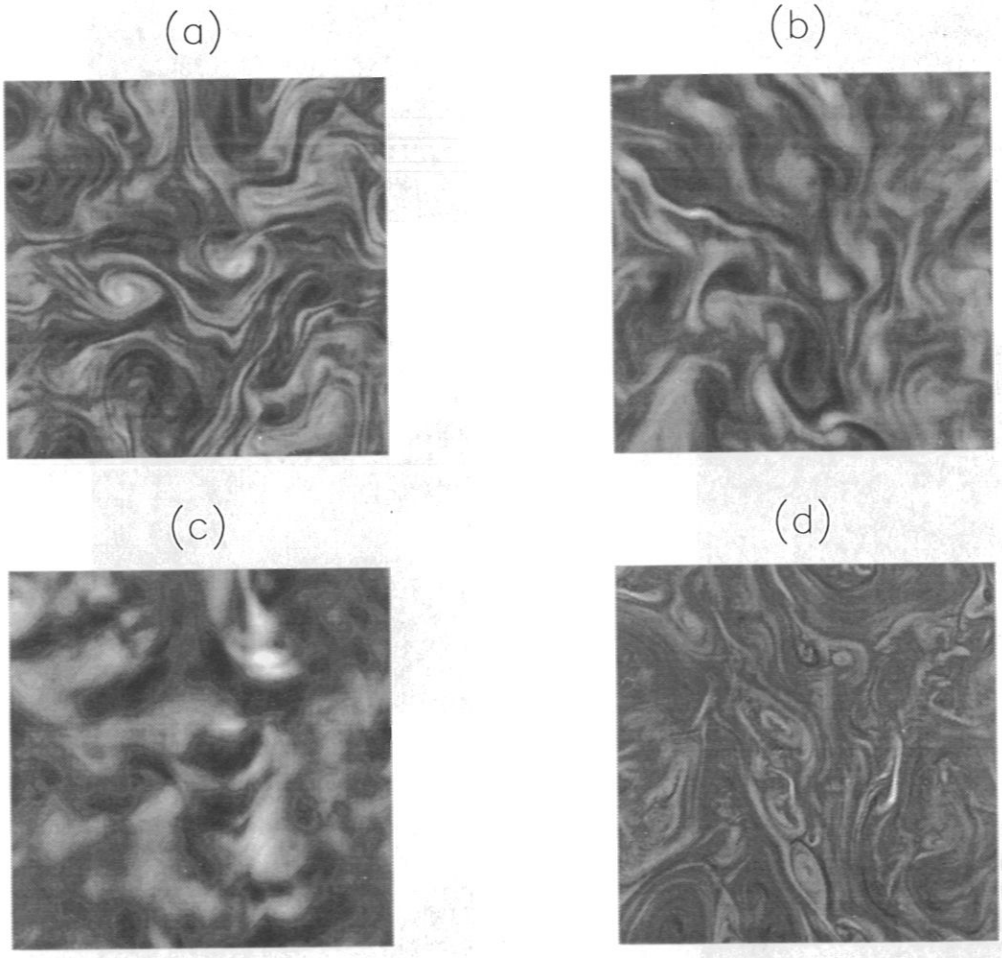

Figure 8: Contour plots of $\widetilde{\Omega}$ ((a) and (b)) and $\widetilde{J}$ ((c) and (d)), for $\mathcal{C} = 5$ in the electrostatic ($\beta = 0.001$) and electromagnetic ($\beta = 10$) regimes, respectively.

$\mathcal{C}$	β	E	E^N/E	E^V/E	E^M/E	U	A	$\tilde{\phi}^2/2$
	0.001	28.0	0.83	0.17	10^{-6}	42.1	10^{-6}	15.3
0.1	0.1	28.3	0.83	0.16	0.0006	42.3	0.009	16.1
	10	13.1	0.83	0.14	0.03	18.8	20.1	8.7
	0.001	6.7	0.61	0.39	10^{-4}	14.0	10^{-7}	3.7
1	0.1	7.6	0.62	0.375	0.005	15.2	0.009	4.4
	10	6.0	0.77	0.14	0.09	7.3	30.1	6.2
	0.001	14.2	0.82	0.18	10^{-5}	18.4	10^{-6}	8.9
5	0.1	23.2	0.86	0.14	0.002	27.9	0.02	22.2
	10	4.4	0.78	0.13	0.09	5.1	13.8	3.7

Table 1: Saturation values in the different regimes.

$\mathcal{C}$	β	E_k	E_k^N	E_k^V	E_k^M	U_k	A_k
	0.001	$k^{-1.7}$	$k^{-1.6}$	$k^{-3.1}$	$k^{-3.4}$	$k^{-1.4}$	$k^{-5.4}$
0.1	0.1	$k^{-1.9}$	$k^{-1.8}$	$k^{-3.1}$	$k^{-3.4}$	$k^{-1.6}$	$k^{-5.5}$
	10	$k^{-3.2}$	$k^{-3.2}$	$k^{-3.5}$	$k^{-4.8}$	$k^{-2.1}$	$k^{-6.0}$
	0.001	$k^{-3.0}$	$k^{-2.8}$	$k^{-3.3}$	$k^{-4.4}$	$k^{-1.5}$	$k^{-6.6}$
1	0.1	$k^{-3.4}$	$k^{-3.0}$	$k^{-3.5}$	$k^{-4.8}$	$k^{-1.9}$	$k^{-6.5}$
	10	$k^{-4.5}$	$k^{-3.8}$	$k^{-5.0}$	$k^{-4.8}$	$k^{-2.1}$	$k^{-6.4}$
	0.001	$k^{-4.0}$	$k^{-4.6}$	$k^{-3.8}$	$k^{-6.0}$	$k^{-2.1}$	$k^{-7.5}$
5	0.1	$k^{-3.7}$	$k^{-4.2}$	$k^{-3.7}$	$k^{-5.8}$	$k^{-2.1}$	$k^{-7.7}$
	10	$k^{-3.2}$	$k^{-3.1}$	$k^{-3.9}$	$k^{-3.1}$	$k^{-2.5}$	$k^{-5.3}$

Table 2: Decay exponents for the invariants and energy components spectra in the different regimes.

to the Hasegawa-Wakatani case for $\mathcal{C} = 0.1$ and $\mathcal{C} = 1$ (see [34]). However, for $\mathcal{C} = 5$ the electromagnetic effects are stronger. Even for $\beta = 0.001$, in the adiabatic regime, the spectral exponents are higher than in the Hasegawa-Wakatani case. As β increases, the spectral exponents of the three invariants and the energy components (E_k^V, E_k^N and E_k^M) increase for $\mathcal{C} = 0.1$ and $\mathcal{C} = 1$. In contrast, the spectral exponents of the energy E_k and its components and the magnetic potential A_k diminish for $\mathcal{C} = 5$, while the spectral exponents of the enstrophy U_k increase. The spectral exponents for both the energy E_k and the magnetic potential A_k in the electromagnetic limit (independent of the value of $\mathcal{C}$) are very different from the ones obtained in 2D MHD turbulence ($-3/2$ and $-7/3$ respectively [19]).

In Fig. 9 the spectra of the energy E_k, the enstrophy U_k and the magnetic potential A_k spectra for different values of β are shown. A different behavior of the spectral exponents

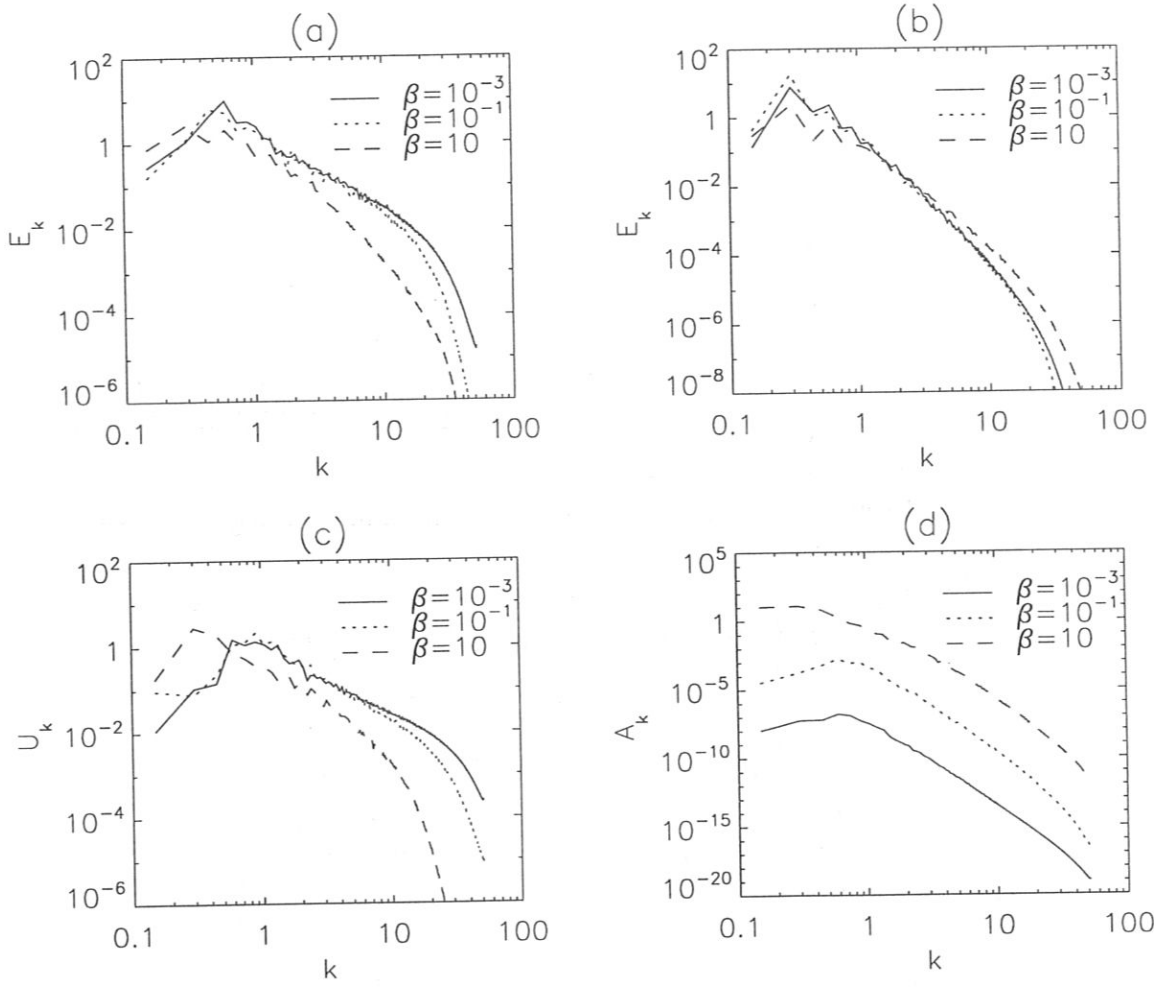

Figure 9: Energy spectra E_k for $\beta = 0.001, 0.1, 10$, $\mathcal{C} = 0.1$ (a) and $\mathcal{C} = 5$ (b). Enstrophy spectra U_k (c) and the magnetic invariant spectra A_k (d) for $\beta = 0.001, 0.1, 10$ and $\mathcal{C} = 1$.

of E_k for $\mathcal{C} = 0.1$ (Fig. 9(a)) and $\mathcal{C} = 5$ (Fig. 9(b)) can be observed. While the curve of E_k for $\beta = 10$ is steeper than the curve for $\beta = 0.001$ for $\mathcal{C} = 0.1$, the opposite happens for $\mathcal{C} = 5$. When the value of β is increased, the enstrophy spectra U_k are steeper for all values of $\mathcal{C}$ (see Fig. 9(c)). The effect of increasing β on the magnetic potential spectra A_k depends on the value of $\mathcal{C}$, (see Fig. 9(d)), but the spectral exponents do not have such strong changes as do the energy spectral exponents. Fig. 10 shows the variation of the spectra of energy components E_k^N, E_k^V and E_k^M by varying β. E_k^N, which is the dominant component of the energy, has a different behavior when β is increased for $\mathcal{C} = 0.1$ and $\mathcal{C} = 5$. E_k^V is not much affected when β is increased, especially for $\mathcal{C} = 0.1$. The magnetic energy component E_k^M also has a steeper curve in the electromagnetic regime ($\beta = 10$) than in the electrostatic regime ($\beta = 0.001$) for $\mathcal{C} = 0.1$. In contrast for $\mathcal{C} = 5$ the effect of increasing β is to make the spectrum of E_k^M less steep.

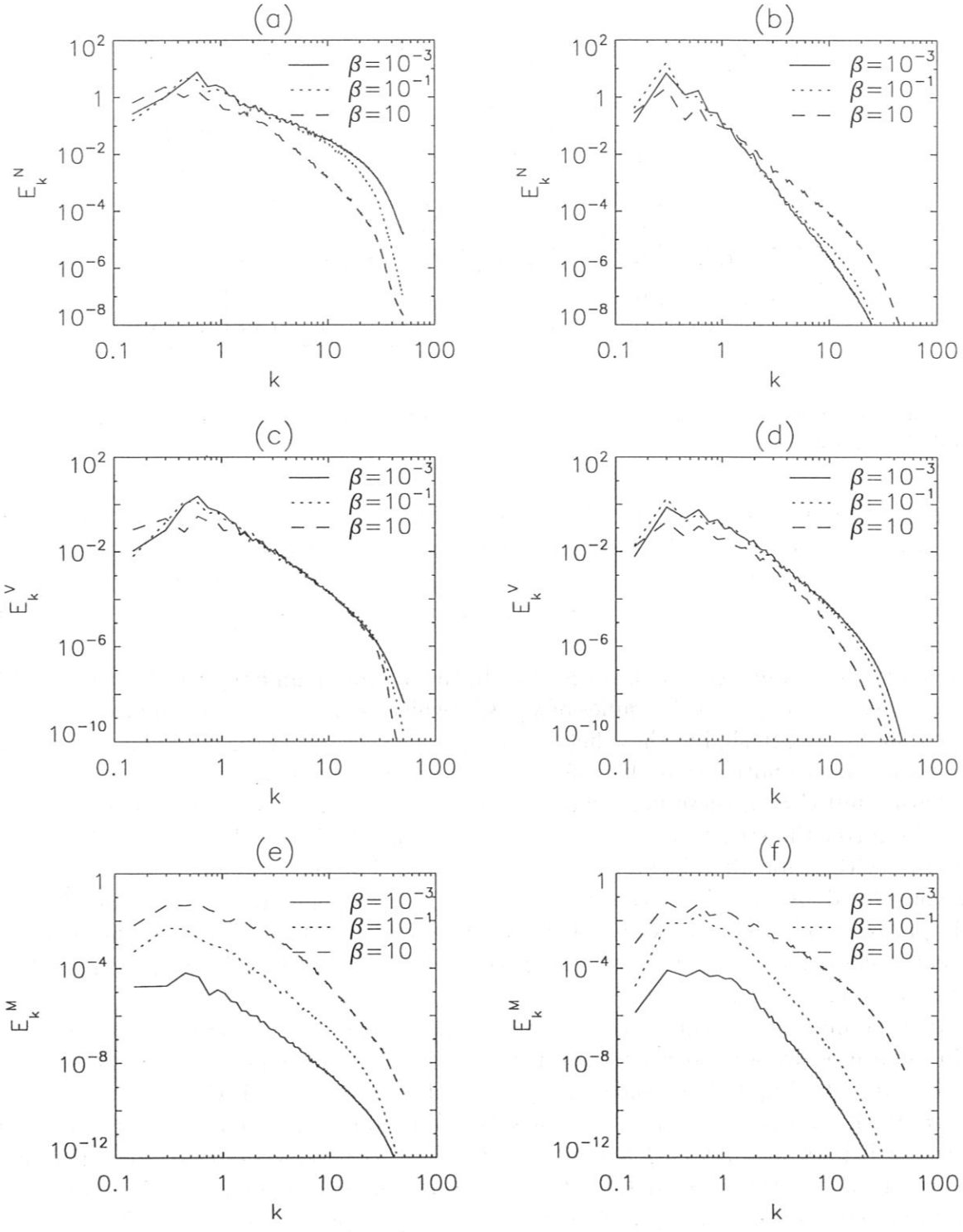

Figure 10: Density spectra E_k^N for $\beta = 0.001, 0.1, 10$, $\mathcal{C} = 0.1$ (a) and $\mathcal{C} = 5$ (b). Kinetic energy spectra E_k^V for $\beta = 0.001, 0.1, 10$, $\mathcal{C} = 0.1$ (c) and $\mathcal{C} = 5$ (d). Magnetic energy spectra E_k^M for $\beta = 0.001, 0.1, 10$, $\mathcal{C} = 0.1$ (e) and $\mathcal{C} = 5$ (f).

$\mathcal{C}$	β	k_m^E	k_m^N	k_m^V	k_m^M	k_m^U	k_m^A	k_m^ϕ
0.1	0.001	1.35	1.43	0.90	0.76	1.58	0.42	0.56
	0.1	1.34	1.41	0.90	0.75	1.57	0.42	0.55
	10	1.10	1.08	1.21	1.11	1.55	0.41	0.46
1	0.001	1.12	1.05	1.21	1.02	1.59	0.69	0.82
	0.1	1.09	1.02	1.19	0.99	1.55	0.67	0.81
	10	0.89	0.78	1.15	1.23	1.25	0.43	0.39
5	0.001	0.53	0.49	0.65	0.67	0.64	0.50	0.48
	0.1	0.45	0.40	0.69	0.80	0.63	0.53	0.37
	10	0.82	0.69	0.99	1.43	1.00	0.48	0.39

Table 3: Average wave-numbers k_m for the invariants, the energy components and $\widetilde{\phi}^2/2$ in the different regimes.

In Table 3 the average values of k are shown for E, E^V, E^M, U, A and $\widetilde{\phi}^2/2$. In the case of the total energy E, for instance, the average k_m^E, is defined as

$$k_m^E = \sqrt{\frac{\sum_k k^2 E_k}{\sum_k E_k}}, \tag{46}$$

with analogous definitions for the other k_m. In the hydrodynamic regime ($\mathcal{C} = 0.1$) and for $\mathcal{C} = 1$, when β is increased the values of k_m^E, k_m^N (which is always the dominant component), k_m^U, k_m^A and k_m^ϕ diminish, i.e. these fields have larger structures in the electromagnetic limit. It is important to notice that this effect is stronger in the case $\mathcal{C} = 1$. In contrast, in the adiabatic limit $\mathcal{C} = 5$, these fields have smaller structures for $\beta = 10$ than for $\beta = 0.001$, as in the latter the structures are already large. From the linear theory the value of $k_{\max}$ increases with β for all values of $\mathcal{C}$ (see Fig. 1(d)). For the runs in which a larger box was considered ($K_0 = 0.0375$) the spectra's maximum k_{SM} and average wave-numbers k_m, had approximately the same values as in the case for $K_0 = 0.15$. Therefore the structures did not become larger. All the other properties of the system remained the same, when a larger box was considered.

Another interesting feature comes from analyzing how the phase-shifts between the main quantities are altered when β is increased and then comparing this with the linear phase-shifts. In Fig. 11 we show the phase-shifts obtained with $\mathcal{C} = 0.1$ in the cases of $\beta = 0.001$ and $\beta = 10$. Fig. 12 show the same functions for $\mathcal{C} = 5$. While in the electrostatic limit $\beta = 0.001$, δ_k^L and δ_k still had some resemblance for $\mathcal{C} = 5$ (compare Figs. 3(a) and 12(a)), in the electromagnetic limit, this resemblance has completely disappeared. The same effect occurs for α_k^L and α_k for $\mathcal{C} = 0.1$ (compare Figs. 2(c) and 11(c)). The other linear and nonlinear phase-shifts are very different in both the electrostatic and electromagnetic limits. Therefore, any small influence that the linear properties still could have on the turbulence in the electrostatic limit practically disappears for $\beta = 10$. This result is expected as the linear growth rates are small in the electromagnetic limit.

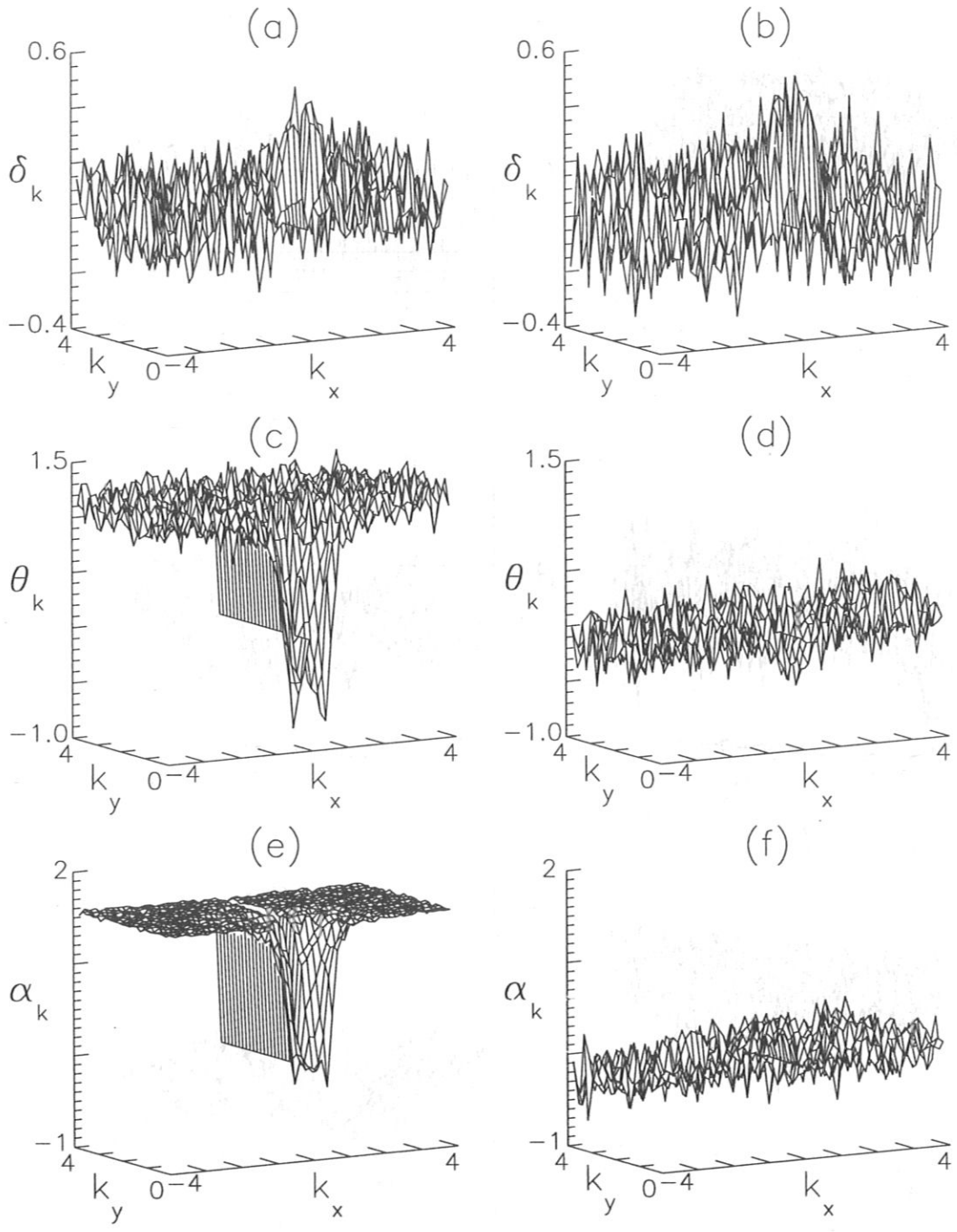

Figure 11: Nonlinear phase-shifts for $\mathcal{C} = 0.1$. $\delta_{\mathbf{k}}$ for $\beta = 0.001$ (a) and $\beta = 10$ (b). $\theta_{\mathbf{k}}$ for $\beta = 0.001$ (c) and $\beta = 10$ (d). $\alpha_{\mathbf{k}}$ for $\beta = 0.001$ (e) and $\beta = 10$ (f)

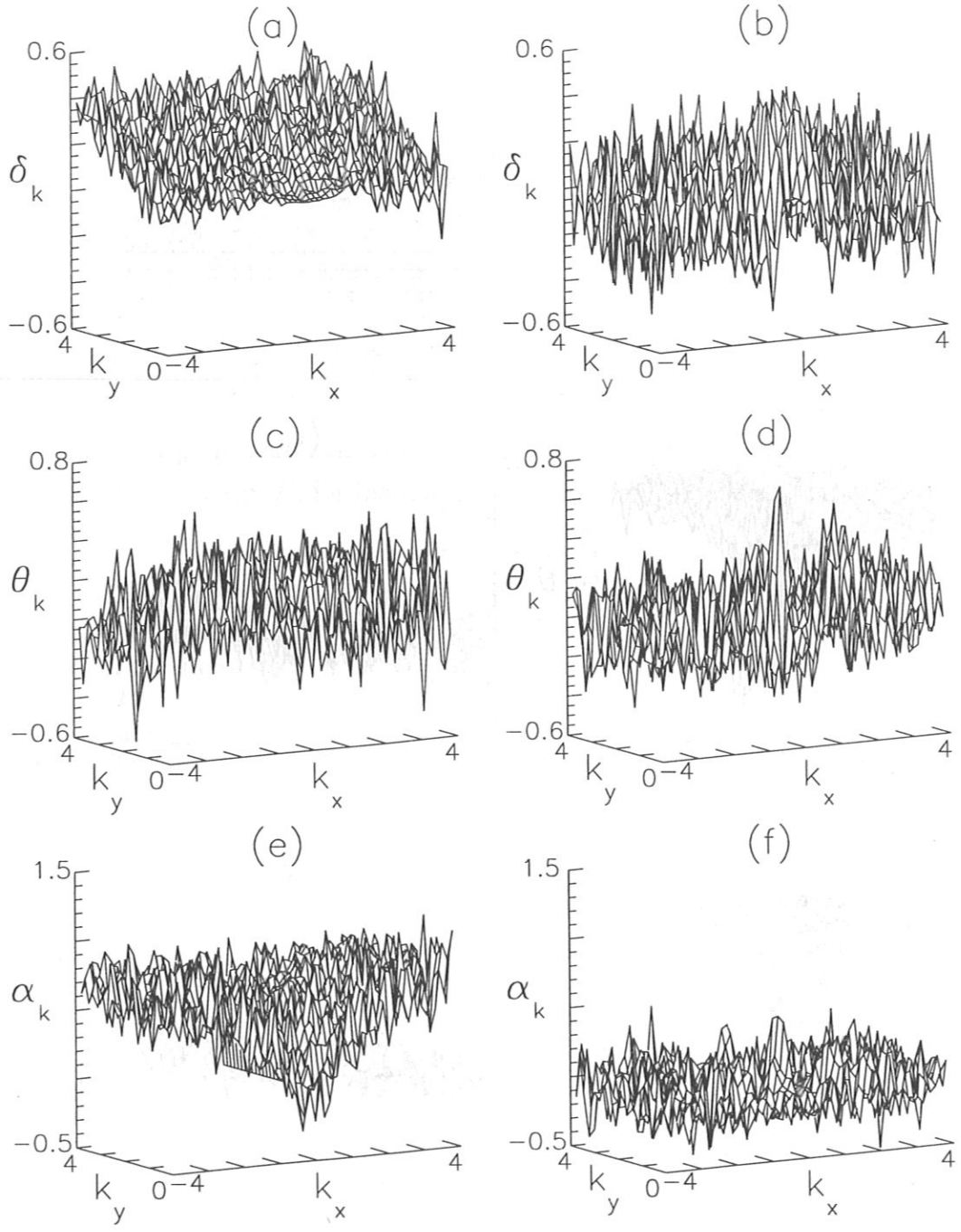

Figure 12: Nonlinear phase-shifts for $\mathcal{C} = 5$. $\delta_{\mathbf{k}}$ for $\beta = 0.001$ (a) and $\beta = 10$ (b). $\theta_{\mathbf{k}}$ for $\beta = 0.001$ (c) and $\beta = 10$ (d). $\alpha_{\mathbf{k}}$ for $\beta = 0.001$ (e) and $\beta = 10$ (f)

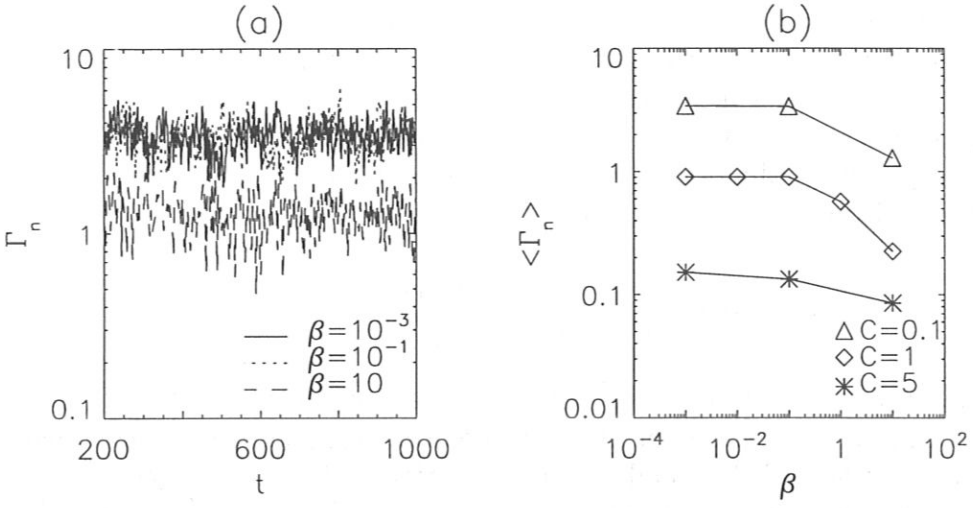

Figure 13: (a) Flux Γ_n for $\mathcal{C} = 0.1$ and $\beta = 0.001, 0.1, 10$ (b). Variation of the average flux $< \Gamma_n >$ with β for $\mathcal{C} = 0.1$, $\mathcal{C} = 1$ and $\mathcal{C} = 5$.

On the other hand, the fluxes are very much affected by the value of β. In particular Γ_n, which is responsible for the transport, diminishes as β increases (see Table 4). This can be interpreted using the linear theory, which shows that the maximum of the linear growth rate $\gamma_{\max}$ diminishes for higher values β (see Fig. 1) with a behavior similar than that of Γ_n, almost constant for $\beta < 1$ and a fast drop for $\beta > 1$ (see Fig. 13).

Bispectral analysis is a standard method for studying turbulence [46, 47, 48]. The bispectrum is equivalent to a two-dimensional Fourier transform of a correlation between two fields. The bispectrum is zero unless there is a phase coupling between the modes. A phase coupling occurs when the two modes k and q are simultaneously present in the signal considered, along with their sum (or difference). The bispectrum between $\tilde{n}$ and $\tilde{\phi}$, for instance, is defined as

$$B^{n\phi}(k,q) = \left\langle \sum_{k=1}^{N} \sum_{q=1}^{N-k} \tilde{\phi}(k)\tilde{\phi}(q)\tilde{n}^*(k+q) \right\rangle, \tag{47}$$

where $\tilde{\phi}(k) = \sum_{k_x} \tilde{\phi}(k_x, k_y)$ and the brackets stand for ensemble averaging (over many realizations). In Figs. 14 and 15 we show the bispectrum between the different variables for $\mathcal{C} = 0.1$ and $\mathcal{C} = 5$ respectively. In the electromagnetic regime ($\beta = 10$) the bispectrum is concentrated in a fewer number of modes than in the electrostatic regime ($\beta = 0.001$), this effect being stronger for $\mathcal{C} = 0.1$. While $B^{\phi\psi}$ and $B^{n\psi}$ increase, $B^{n\phi}$ diminishes as β increases for $\mathcal{C} = 0.1$ and $\mathcal{C} = 5$. This reflects the fact that in the hydrodynamic regime for higher β the quantities follow ψ; and in the adiabatic regime by increasing β the adiabaticity becomes poorer, as can be seen in the contour plots (Figs. 5 and 7). The largest values of the bispectra are obtained for $\beta = 0.001$ (electrostatic limit) in $B^{n\phi}$. Therefore, even though for $\mathcal{C} = 0.1$ $\tilde{n}$ does not mimic $\tilde{\phi}$, as happens for $\mathcal{C} = 5$, there is a

strong phase coupling between $\tilde{\phi}$ and $\tilde{n}$. In the electromagnetic limit $\beta = 10$, for $\mathcal{C} = 0.1$, $B^{\phi\psi}$ has larger values than $B^{n\psi}$, the opposite happening for $\mathcal{C} = 5$, reflecting once more the similarities that occur between the different contour plots for $\beta = 10$.

A quantity related to the bispectrum is the bicoherence. The bicoherence is a measure of the amount of phase coupling that occurs in the signal considered and is defined as the normalized squared bispectrum. The bicoherence between $\tilde{n}$ and $\tilde{\phi}$, for instance, is defined as

$$b^{n\phi}(k,q) = \frac{\left(B^{n\phi}(k,q)\right)^2}{\sum_{k,q}\left(B^{n\phi}(k,q)\right)^2}. \tag{48}$$

The bicoherence takes a value close to unity when a nonlinear (quadratic) interaction takes place, showing a high degree of phase coherence. A value of the bicoherence near zero suggests an absence of the quadratic nonlinearity and a low degree of coherence, indicating that any waves present are probably spontaneously excited independent modes rather than coupled modes [47]. The bicoherence between the different quantities in both the electrostatic and the electromagnetic regime for $\mathcal{C} = 0.1, 1, 5$ was calculated. In Fig. 16 we show the bicoherence between the different variables for $\mathcal{C} = 5$ in the electrostatic and the electromagnetic limits. For all values of $\mathcal{C}$ and β, the bicoherence was low, with its maximum value (0.2) occurring, as expected, between $\tilde{\phi}$ and $\tilde{n}$ for $\mathcal{C} = 5$ and $\beta = 0.001$. The low values of the bicoherence in all cases are in agreement with the fact that no long lived coherent structures were observed. When the turbulence exhibits coherent structures a phase coupling can be expected [48]. For $\mathcal{C} = 0.1$ and $\mathcal{C} = 1$ the increase of β does not affect greatly the values of the bicoherence; the maximum value of $b^{n\phi}$ increases from 0.05 to 0.08. The maximum values of $b^{n\psi}$ and $b^{\phi\psi}$ remained approximately constant (0.05) for $\mathcal{C} = 0.1$ and increasing values of β (0.001 - 10). On the other hand, for $\mathcal{C} = 5$ the maximum of all bicoherence diminish strongly in the electromagnetic regime. Especially $b^{n\phi}$ has its maximum strongly diminished as β varies from 0.001 to 10 (Fig. 16). This once more reflects the fact that in the electromagnetic regime the system is less adiabatic than in the electrostatic regime.

5 Linear and Nonlinear Spectral Transfer

The dynamical quantities which reveal the most information about the direction of cause and effect in a complicated turbulent system are the rates of transfer of invariants or pieces of invariants among different parts of the system. Linear transfer refers to exchanges between different dependent variables within each Fourier component or mode $\mathbf{k}$; e.g. the transfer of fluctuation free energy between density and potential fluctuations mediated by the dissipative coupling through $\nabla_{\parallel}\tilde{J}$ in the equations for $\tilde{n}$ and $\nabla_{\perp}^2\tilde{\phi}$. Nonlinear transfer, also called spectral transfer, refers to exchanges between different modes. This can occur within a given dependent variable, as e.g. for $\mathbf{E} \times \mathbf{B}$ transferring density fluctuations free energy between two modes with different $\mathbf{k}$. With magnetic fluctuations present this mode-mode transfer can also occur between different dependent variables, as we shall see.

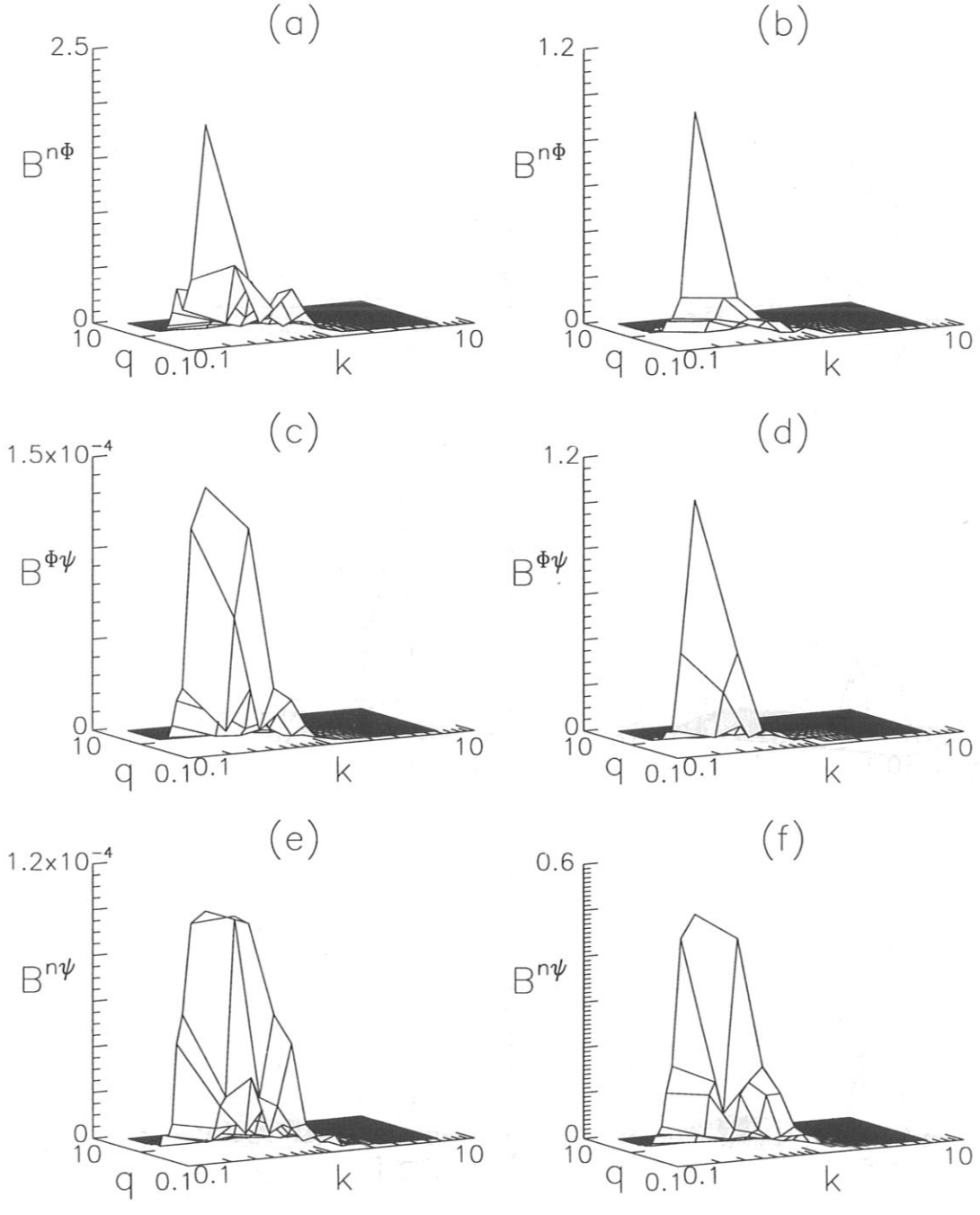

Figure 14: Bispectra for $\mathcal{C} = 0.1$. $B^{n\phi}$ for $\beta = 0.001$ (a) and $\beta = 10$ (b). $B^{\phi\psi}$ for $\beta = 0.001$ (c) and $\beta = 10$ (d). $B^{n\psi}$ for $\beta = 0.001$ (e) and $\beta = 10$ (f).

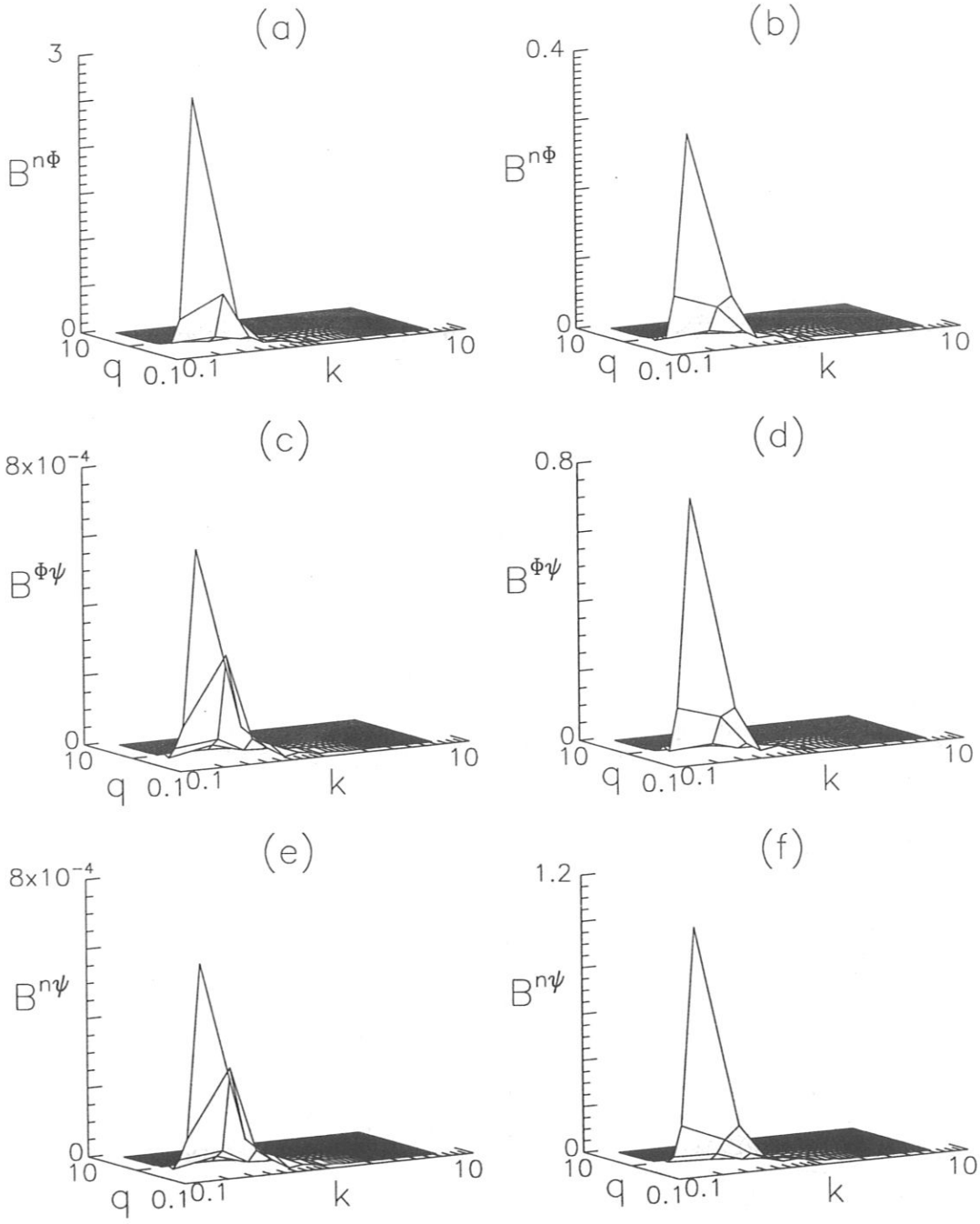

Figure 15: Bispectra for $\mathcal{C} = 5$. $B^{n\phi}$ for $\beta = 0.001$ (a) and $\beta = 10$ (b). $B^{\phi\psi}$ for $\beta = 0.001$ (c) and $\beta = 10$ (d). $B^{n\psi}$ for $\beta = 0.001$ (e) and $\beta = 10$ (f).

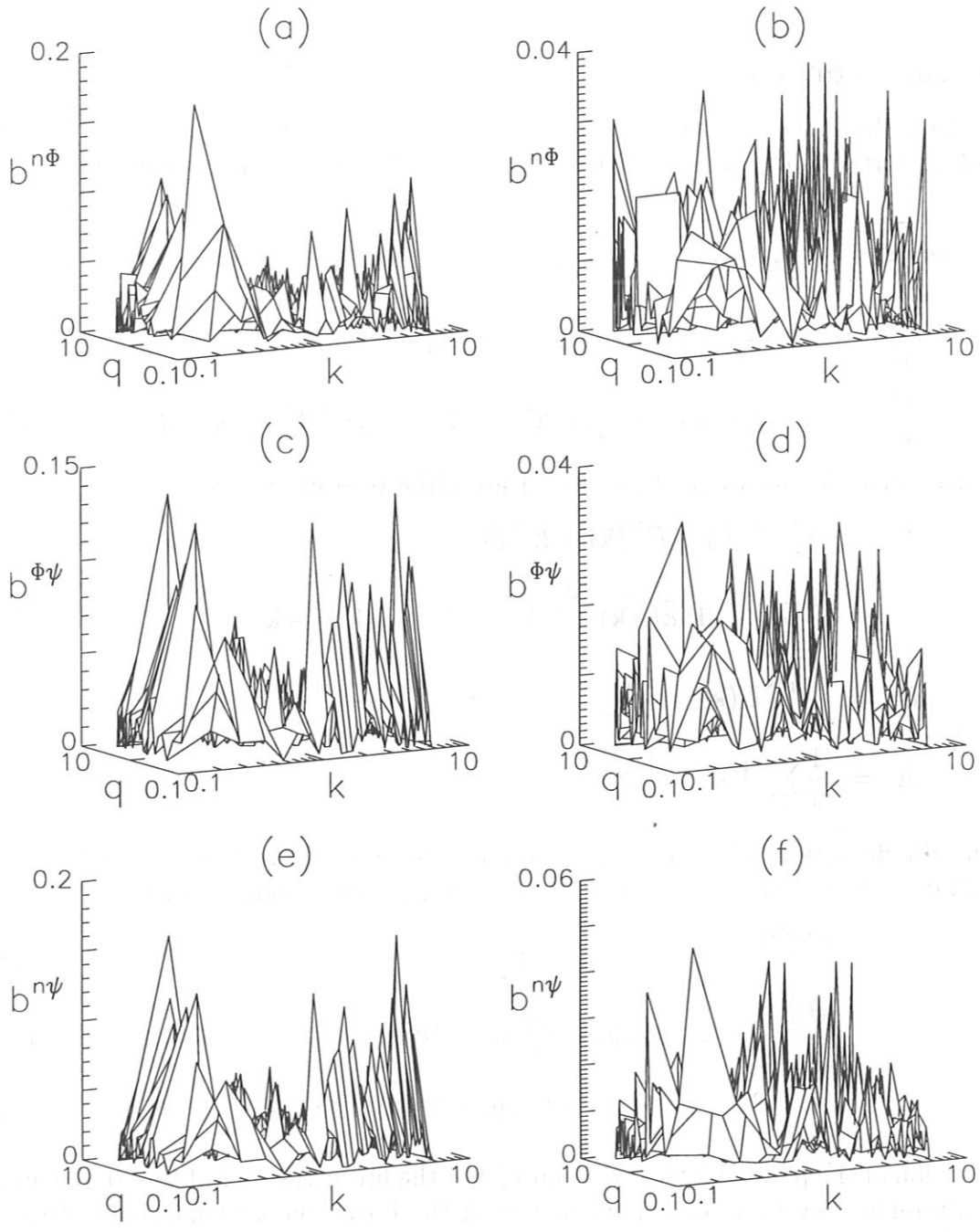

Figure 16: Bicoherence for $\mathcal{C} = 5$. $b^{n\phi}$ for $\beta = 0.001$ (a) and $\beta = 10$ (b). $b^{\phi\psi}$ for $\beta = 0.001$ (c) and $\beta = 10$ (d). $b^{n\psi}$ for $\beta = 0.001$ (e) and $\beta = 10$ (f).

Such transfer analysis has proven very useful in understanding cascade phenomena in neutral fluid [49] and electrostatic drift-wave [34] turbulence. We now apply it to the electromagnetic drift-wave system.

5.1 Linear Transfer

We now obtain the linear transfer of energy, enstrophy and magnetic potential between the dependent variables $\tilde{\phi}$, $\tilde{n}$ and $\tilde{\psi}$ within a mode $\mathbf{k}$. The linearized equations in Fourier space are

$$\frac{\partial \tilde{\Omega}(\mathbf{k})}{\partial t} = iK_{\parallel}\tilde{J}(\mathbf{k}) - \mu k^4 \tilde{\Omega}(\mathbf{k}), \tag{49}$$

$$\frac{\partial \tilde{n}(\mathbf{k})}{\partial t} = -ik_y\tilde{\phi}(\mathbf{k}) + iK_{\parallel}\tilde{J}(\mathbf{k}) - \mu k^4 \tilde{n}(\mathbf{k}), \tag{50}$$

$$\frac{\partial \tilde{\psi}(\mathbf{k})}{\partial t} = -ik_y\tilde{\psi}(\mathbf{k}) + iK_{\parallel}\left(\tilde{n}(\mathbf{k}) - \tilde{\phi}(\mathbf{k})\right) - \eta_* \beta \tilde{J}(\mathbf{k}) - \mu k^4 \tilde{\psi}(\mathbf{k}). \tag{51}$$

In Fourier space the invariants E, U and A are given respectively by

$$\begin{aligned} E &= \sum_{\mathbf{k}} E^V(\mathbf{k}) + E^N(\mathbf{k}) + E^M(\mathbf{k}) \\ &= \frac{1}{2}\sum_{\mathbf{k}} -\tilde{\Omega}(\mathbf{k})\tilde{\phi}(-\mathbf{k}) + \tilde{n}(\mathbf{k})\tilde{n}(-\mathbf{k}) + \tilde{J}(\mathbf{k})\tilde{\psi}(-\mathbf{k}), \end{aligned} \tag{52}$$

$$U = \frac{1}{2}\sum_{\mathbf{k}} U(\mathbf{k}) = \frac{1}{2}\sum_{\mathbf{k}} \left(\tilde{n}(\mathbf{k}) - \tilde{\Omega}(\mathbf{k})\right)\left(\tilde{n}(-\mathbf{k}) - \tilde{\Omega}(-\mathbf{k})\right), \tag{53}$$

$$A = \frac{1}{2}\sum_{\mathbf{k}} A(\mathbf{k}) = \frac{1}{2}\sum_{\mathbf{k}} \tilde{\psi}(\mathbf{k})\tilde{\psi}(-\mathbf{k}). \tag{54}$$

By using the definitions of each of the energy contributions given in equation (52) and equations (49) - (51) we obtain the linear transfer of the energy components:

$$\frac{\partial E_L^V(\mathbf{k})}{\partial t} = -\Gamma_p^V(\mathbf{k}) - \mathcal{D}_V^E(\mathbf{k}), \tag{55}$$

$$\frac{\partial E_L^N(\mathbf{k})}{\partial t} = \Gamma_n(\mathbf{k}) - \Gamma_p^N(\mathbf{k}) - \mathcal{D}_N^E(\mathbf{k}), \tag{56}$$

$$\frac{\partial E_L^M(\mathbf{k})}{\partial t} = \Gamma_p^N(\mathbf{k}) + \Gamma_p^V(\mathbf{k}) - \Gamma_r(\mathbf{k}) - \mathcal{D}_M^E(\mathbf{k}). \tag{57}$$

The contribution of the parallel fluxes (Γ_p^N and Γ_p^V) to the linear transfer of the total energy E is zero, although they have an important role in the linear energy transfer for each of the energy components.

The linear transfer for the enstrophy U and the magnetic potential A can be obtained in a similar way and are respectively

$$\frac{\partial U_L(\mathbf{k})}{\partial t} = \Gamma_n(\mathbf{k}) - \mathcal{D}^U(\mathbf{k}), \tag{58}$$

$\mathcal{C}$	β	Γ_n	Γ_p^N	Γ_p^V	Γ_r	Γ_a	Γ_d	$\mathcal{D}_N^E$	$\mathcal{D}_V^E$	$\mathcal{D}_M^E$	$\mathcal{D}^U$	$\mathcal{D}^A$
	0.001	3.4	1.9	-0.03	0.9	10^{-4}	-10^{-5}	1.2	0.03	10^{-7}	2.7	10^{-10}
0.1	0.1	3.3	1.9	-0.03	0.9	0.25	-0.008	1.1	0.03	10^{-5}	2.6	10^{-5}
	10	1.3	0.2	0.005	0.5	7.1	-0.004	0.2	0.04	0.007	1.1	0.07
	0.001	0.9	0.7	-0.03	0.3	10^{-4}	10^{-6}	0.04	0.03	10^{-6}	0.6	10^{-7}
1	0.1	0.9	0.9	-0.05	0.4	0.06	10^{-4}	0.04	0.04	10^{-4}	0.7	0.01
	10	0.2	0.02	-0.01	0.08	1.5	-0.002	0.03	0.01	0.01	0.2	0.3
	0.001	0.1	0.1	-0.01	0.07	-10^{-4}	-10^{-6}	0.003	0.01	10^{-6}	0.1	10^{-10}
5	0.1	0.1	0.1	-0.02	0.06	-0.02	10^{-4}	0.003	0.06	10^{-5}	0.1	10^{-5}
	10	0.09	0.01	-0.02	0.02	0.7	-0.002	0.02	0.006	0.02	0.08	0.09

Table 4: Total values of the linear transfers in the different regimes.

$$\frac{\partial A_L(\mathbf{k})}{\partial t} = \Gamma_a(\mathbf{k}) - \Gamma_d(\mathbf{k}) - \mathcal{D}^A(\mathbf{k}). \tag{59}$$

The fluxes and dissipation terms in Fourier space are

$$\Gamma_p^V(\mathbf{k}) = -\frac{i}{2}K_\parallel\left(\tilde{\phi}(\mathbf{k})\tilde{J}(-\mathbf{k}) - \tilde{\phi}(-\mathbf{k})\tilde{J}(\mathbf{k})\right), \tag{60}$$

$$\Gamma_p^N(\mathbf{k}) = \frac{i}{2}K_\parallel\left(\tilde{n}(\mathbf{k})\tilde{J}(-\mathbf{k}) - \tilde{n}(-\mathbf{k})\tilde{J}(\mathbf{k})\right), \tag{61}$$

$$\Gamma_n(\mathbf{k}) = \frac{i}{2}k_y\left(\tilde{n}(\mathbf{k})\tilde{\phi}(-\mathbf{k}) - \tilde{n}(-\mathbf{k})\tilde{\phi}(\mathbf{k})\right), \tag{62}$$

$$\Gamma_r(\mathbf{k}) = \eta_*\beta\tilde{J}(\mathbf{k})\tilde{J}(-\mathbf{k}), \tag{63}$$

$$\Gamma_a(\mathbf{k}) = \frac{i}{2}K_\parallel\left(\left(\tilde{\phi}(\mathbf{k}) - \tilde{n}(\mathbf{k})\right)\tilde{\psi}(-\mathbf{k}) - \left(\tilde{\phi}(-\mathbf{k}) - \tilde{n}(-\mathbf{k})\right)\tilde{\psi}(\mathbf{k})\right), \tag{64}$$

$$\Gamma_d(\mathbf{k}) = \eta_*\beta\tilde{\psi}(\mathbf{k})\tilde{J}(-\mathbf{k}), \tag{65}$$

$$\begin{aligned}\mathcal{D}^E(\mathbf{k}) &= D_N^E(\mathbf{k}) + D_V^E(\mathbf{k}) + D_M^E(\mathbf{k}) \\ &= \mu k^4\left(\tilde{n}(\mathbf{k})\tilde{n}(-\mathbf{k}) - \tilde{\Omega}(\mathbf{k})\tilde{\phi}(-\mathbf{k}) + k^4\tilde{\psi}(\mathbf{k})\tilde{J}(-\mathbf{k})\right),\end{aligned} \tag{66}$$

$$\mathcal{D}^U(\mathbf{k}) = \mu k^4\left(\tilde{n}(\mathbf{k}) - \tilde{\Omega}(\mathbf{k})\right)\left(\tilde{n}(-\mathbf{k}) - \tilde{\Omega}(-\mathbf{k})\right), \tag{67}$$

$$\mathcal{D}^A(\mathbf{k}) = \mu k^4\tilde{\psi}(\mathbf{k})\tilde{\psi}(-\mathbf{k}). \tag{68}$$

In Figs. 17 and 18 the linear transfer is shown for $\mathcal{C} = 0.1$ and $\mathcal{C} = 5$ in the electrostatic and electromagnetic regimes. The fluxes are shown as a function of $k = |\mathbf{k}|$. In Table 4 the total values of the linear fluxes and dissipation terms are given in all regimes. In Fig. 23, the schematic direction of the linear and nonlinear transfers is shown.

Figs. 17 and 18 and Table 4, show that the dominant contribution of the linear transfer is given by Γ_n, which is the source of energy. The maximum of $\Gamma_n(k)$ is located at a $k \simeq 0.7$ for $\mathcal{C} = 0.1$ (Fig. 17), which is very near the maximum of the energy spectrum E_k (Fig.

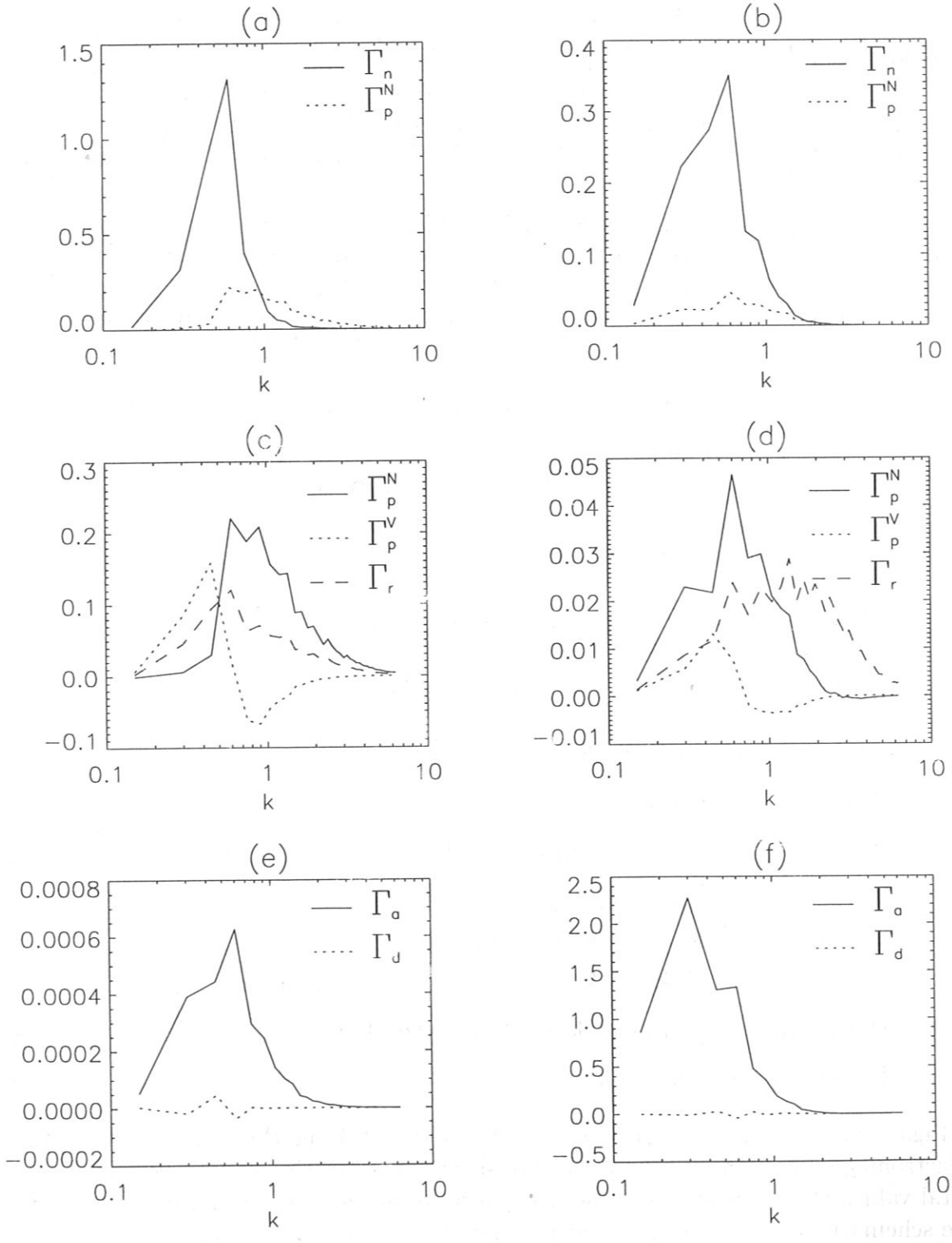

Figure 17: Linear fluxes for $\mathcal{C} = 0.1$, with $\beta = 0.001$ ((a), (c) and (e)) and $\beta = 10$ ((b), (d) and (f))

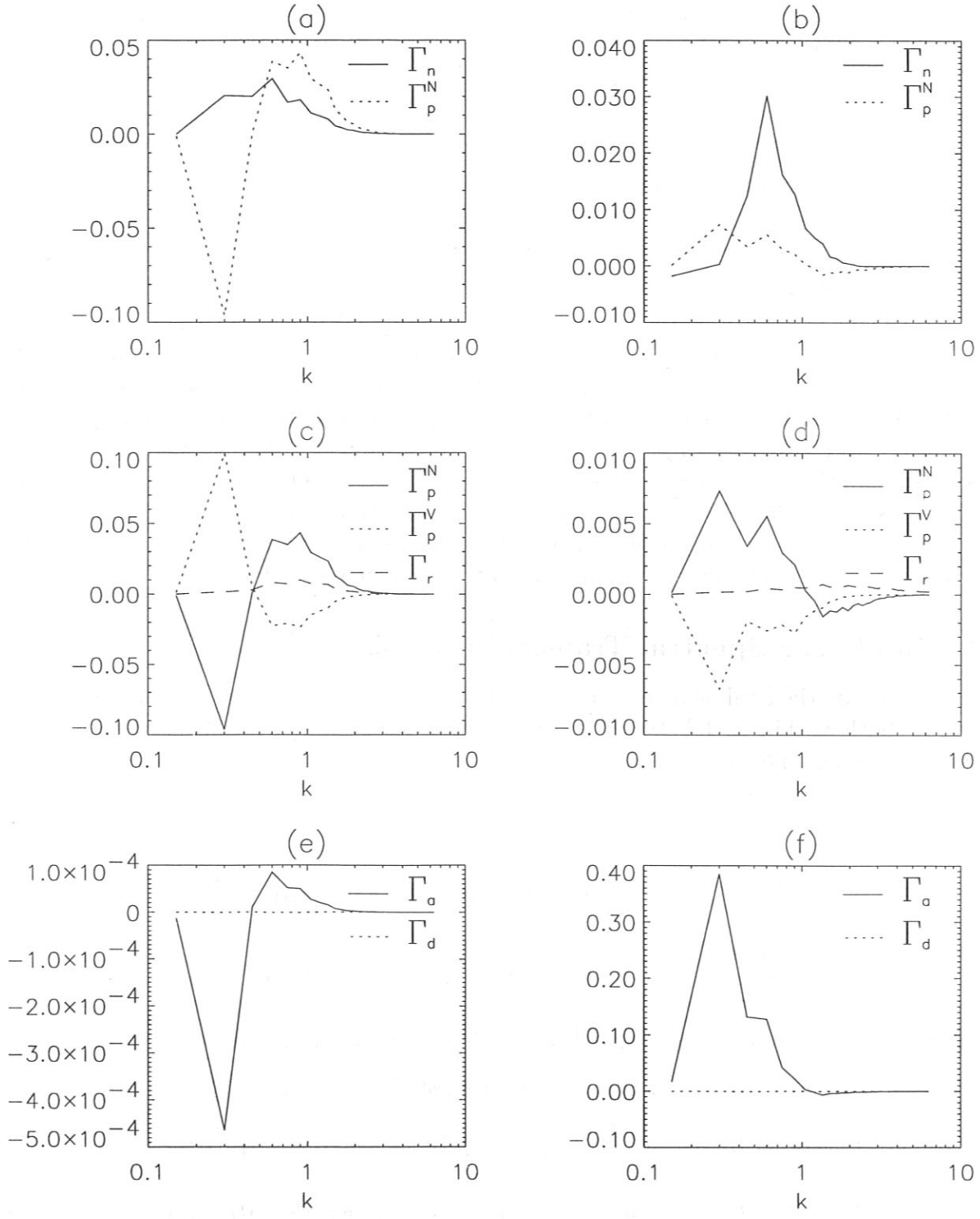

Figure 18: Linear fluxes for $\mathcal{C} = 5$, with $\beta = 0.001$ ((a), (c) and (e)) and $\beta = 10$ ((b), (d) and (f))

9). By contrast, for $\mathcal{C} = 5$ the maximum of $\Gamma_n(k)$ is located at $k \simeq 0.5$ and the maximum of E_k at $k \simeq 0.3$ (compare Figs. 18 and 9).

Another important contribution comes from $\Gamma_p^n(k)$, which is responsible for the linear transfer from $\widetilde{n}$ to $\widetilde{\psi}$. When β increases, $\Gamma_p^n(k)$ is located at smaller values of k. For $\mathcal{C} = 5$ and $\beta = 0.001$, $\Gamma_p^n(k)$ has a negative contribution in the smaller values of k, which means that in this case the linear transfer is in the other direction - from $\widetilde{\psi}$ to $\widetilde{n}$) - (Fig. 18). This effect disappears when β is increased (Fig. 18). $\Gamma_p^V(k)$ is responsible for the linear transfer between $\widetilde{\phi}$ and $\widetilde{\psi}$. $\Gamma_p^V(k)$ is (in most cases) positive for the smaller values of k (linear transfer from $\widetilde{\phi}$ to $\widetilde{\psi}$) and negative for the higher values of k (linear transfer from $\widetilde{\psi}$ to $\widetilde{\phi}$), as can be seen in Figs. 17 and 18. The total contribution of $\Gamma_p^V(k)$ is (in most cases) negative, the main effect being therefore the transfer from $\widetilde{\phi}$ to $\widetilde{\psi}$ (see Table 4). It is interesting to note that in the electromagnetic limit, for $\mathcal{C} = 0.1$, the total contribution of $\Gamma_p^V(k)$ is positive (see Table 4), while for $\mathcal{C} = 5$, $\Gamma_p^V(k)$ is negative in the whole spectrum (Fig. 18). By comparing Figs. 17 and 18, one notices that $\Gamma_r(k)$ (responsible for the resistive dissipation) has a more important role for $\mathcal{C} = 0.1$ than for $\mathcal{C} = 5$. By increasing β, Γ_r is dislocated for higher values of k. $\Gamma_a(k)$, which is the source of the magnetic potential, has a strong dependence with β, with its values increasing dramatically with increasing β and it maximum being dislocated to much smaller values of k.

5.2 Nonlinear Spectral Transfer Analysis

We now compute the nonlinear spectral transfer of the different invariants between different **k**-modes, both within and between the dependent variables. By considering only the nonlinear terms of the equations, we obtain for the nonlinear energy transfer:

$$\frac{\partial E^V(\mathbf{k})}{\partial t} = \sum_{\mathbf{q}} \left(T^V(\mathbf{k} \leftarrow \mathbf{q}) + T_1^{VM}(\mathbf{k} \leftarrow \mathbf{q}) \right), \tag{69}$$

$$\frac{\partial E^N(\mathbf{k})}{\partial t} = \sum_{\mathbf{q}} \left(T^N(\mathbf{k} \leftarrow \mathbf{q}) + T_1^{NM}(\mathbf{k} \leftarrow \mathbf{q}) \right), \tag{70}$$

$$\frac{\partial E^M(\mathbf{k})}{\partial t} = \sum_{\mathbf{q}} \left(T_2^{VM}(\mathbf{k} \leftarrow \mathbf{q}) + T_2^{NM}(\mathbf{k} \leftarrow \mathbf{q}) \right), \tag{71}$$

where the spectral transfers of energy from mode **q** to mode **k** are given by

$$T^V(\mathbf{k} \leftarrow \mathbf{q}) = 2\,(k_x q_y - q_x k_y)\,\mathrm{Re}\left(\widetilde{\phi}(-\mathbf{k})\widetilde{\Omega}(\mathbf{k}-\mathbf{q})\widetilde{\phi}(\mathbf{q})\right), \tag{72}$$

$$T_1^{VM}(\mathbf{k} \leftarrow \mathbf{q}) = -2\frac{1}{\beta}\,(k_x q_y - q_x k_y)\,\mathrm{Re}\left(\widetilde{\phi}(-\mathbf{k})\widetilde{\psi}(\mathbf{k}-\mathbf{q})\widetilde{J}(\mathbf{q})\right), \tag{73}$$

$$T_2^{VM}(\mathbf{k} \leftarrow \mathbf{q}) = -2\frac{1}{\beta}\,(k_x q_y - q_x k_y)\,\mathrm{Re}\left(\widetilde{J}(-\mathbf{k})\widetilde{\psi}(\mathbf{k}-\mathbf{q})\widetilde{\phi}(\mathbf{q})\right), \tag{74}$$

$$T^N(\mathbf{k} \leftarrow \mathbf{q}) = 2\,(k_x q_y - q_x k_y)\,\mathrm{Re}\left(\widetilde{n}(-\mathbf{k})\widetilde{\phi}(\mathbf{k}-\mathbf{q})\widetilde{n}(\mathbf{q})\right), \tag{75}$$

$$T_1^{NM}(\mathbf{k} \leftarrow \mathbf{q}) = 2\frac{1}{\beta}\,(k_x q_y - q_x k_y)\,\mathrm{Re}\left(\widetilde{n}(-\mathbf{k})\widetilde{\psi}(\mathbf{k}-\mathbf{q})\widetilde{J}(\mathbf{q})\right), \tag{76}$$

$$T_2^{NM}(\mathbf{k} \leftarrow \mathbf{q}) = 2\frac{1}{\beta}(k_x q_y - q_x k_y)\,\mathrm{Re}\left(\tilde{J}(-\mathbf{k})\tilde{\psi}(\mathbf{k}-\mathbf{q})\tilde{n}(\mathbf{q})\right). \quad (77)$$

It is important to understand how this transfer occurs. By considering now the mode $\mathbf{q}$, we have

$$\frac{\partial E^V(\mathbf{q})}{\partial t} = -\sum_{\mathbf{q}}\left(T^V(\mathbf{k} \leftarrow \mathbf{q}) + T_2^{VM}(\mathbf{k} \leftarrow \mathbf{q})\right), \quad (78)$$

$$\frac{\partial E^N(\mathbf{q})}{\partial t} = -\sum_{\mathbf{q}}\left(T^N(\mathbf{k} \leftarrow \mathbf{q}) + T_2^{NM}(\mathbf{k} \leftarrow \mathbf{q})\right), \quad (79)$$

$$\frac{\partial E^M(\mathbf{q})}{\partial t} = -\sum_{\mathbf{q}}\left(T_1^{VM}(\mathbf{k} \leftarrow \mathbf{q}) + T_1^{NM}(\mathbf{k} \leftarrow \mathbf{q})\right). \quad (80)$$

Therefore, the purely kinetic and density transfer terms are transferred in a direct way (between different modes of the same fluctuation field), while the mixed magnetic-kinetic and magnetic-density terms are nonlinear transfers between modes of $\tilde{n}$ and $\tilde{\psi}$ or $\tilde{\phi}$ and $\tilde{\psi}$. That is, the $\mathbf{E} \times \mathbf{B}$ transfer remains within a given dependent variable, but the magnetic transfer occurs between different dependent variables. Each of the nonlinear transfer mixed terms (T_1^{VM},T_2^{VM},T_1^{NM} and T_2^{NM}) is not symmetric by itself, a sum must be defined in order to obtain transfer terms with a definition equivalent to the other transfer terms. T^{VM} and T^{NM} are defined respectively as $T^{VM}(\mathbf{k} \leftarrow \mathbf{q}) = T_1^{VM}(\mathbf{k} \leftarrow \mathbf{q}) + T_2^{VM}(\mathbf{k} \leftarrow \mathbf{q})$ and $T^{NM}(\mathbf{k} \leftarrow \mathbf{q}) = T_1^{NM}(\mathbf{k} \leftarrow \mathbf{q}) + T_2^{NM}(\mathbf{k} \leftarrow \mathbf{q})$. The resulting effect of the mixed transfer terms is then given by T^{VM} and T^{NM}, which then define the character of the nonlinear transfer. A schematic form of the nonlinear and the linear transfers of energy can be found in Fig. 23.

We are also interested in the spectral transfer of the enstrophy U (see equation (53)) and the magnetic potential A (see equation (54)). We obtain:

$$\begin{aligned}\frac{\partial U(\mathbf{k})}{\partial t} &= \sum_{\mathbf{q}} T^U(\mathbf{k} \leftarrow \mathbf{q}) \\ &= \sum_{\mathbf{q}} 2\,(k_x q_y - q_x k_y)\,\mathrm{Re}\left(\left(\tilde{n}(-\mathbf{k}) - \tilde{\Omega}(-\mathbf{k})\right)\tilde{\phi}(\mathbf{k}-\mathbf{q})\left(\tilde{n}(\mathbf{q}) - \tilde{\Omega}(\mathbf{q})\right)\right), \quad (81) \\ \frac{\partial A(\mathbf{k})}{\partial t} &= \sum_{\mathbf{q}} T^A(\mathbf{k} \leftarrow \mathbf{q}) \\ &= \sum_{\mathbf{q}} 2\,(k_x q_y - q_x k_y)\,\mathrm{Re}\left(\tilde{\psi}(-\mathbf{k})\left(\tilde{\phi}(\mathbf{k}-\mathbf{q}) - \tilde{n}(\mathbf{k}-\mathbf{q})\right)\tilde{\psi}(\mathbf{q})\right). \quad (82)\end{aligned}$$

In Figs. 19 and 20 the nonlinear transfer of the energy components are shown for $\mathcal{C} = 0.1$ and $\mathcal{C} = 5$, respectively. In both Figs. the electrostatic and the electromagnetic regimes are shown. In Figs. 21 and 22 the nonlinear transfer of the three invariants of the system (E, U and A) is shown in the electrostatic and the electromagnetic regimes for $\mathcal{C} = 0.1$ and $\mathcal{C} = 5$ respectively. In Figs. 19 - 22, contours of $T(\mathbf{k} \leftarrow \mathbf{q})$ are shown only where it is positive, since by definition the nonlinear transfer functions are anti-symmetric about the

$\mathcal{C}$	β	$T^N_{\max}$	$T^V_{\max}$	$T^{NM}_{\max}$	$T^{VM}_{\max}$	$T^E_{\max}$	$T^U_{\max}$	$T^A_{\max}$
	0.001	1.29	0.23	10^{-6}	10^{-6}	1.16	2.03	10^{-8}
0.1	0.1	1.45	0.30	0.001	10^{-4}	1.15	2.24	10^{-4}
	10	0.24	0.02	0.01	0.006	0.23	0.33	0.19
	0.001	0.12	0.08	10^{-5}	10^{-5}	0.06	0.33	10^{-8}
1	0.1	0.19	0.13	0.001	0.001	0.07	0.39	10^{-4}
	10	0.03	0.004	0.007	0.003	0.03	0.05	0.10
	0.001	0.38	0.11	10^{-5}	10^{-5}	0.27	0.60	10^{-9}
5	0.1	0.22	0.09	0.001	0.001	0.17	0.31	10^{-4}
	10	0.02	0.003	0.005	0.002	0.02	0.02	0.06

Table 5: Maximum values of the nonlinear transfers in the different regimes.

$\mathcal{C}$	β	T^N	T^V	T^{NM}	T^{VM}	T^E	T^U	T^A
	0.001	direct	inverse	mixed	direct	direct	direct	direct
0.1	0.1	direct	inverse	mixed	mixed	direct	direct	direct
	10	direct	inverse	direct	direct	direct	direct	direct
	0.001	direct	inverse	mixed	mixed	direct	direct	mixed
1	0.1	direct	inverse	mixed	mixed	direct	direct	direct
	10	direct	mixed	direct	direct	direct	direct	direct
	0.001	direct	inverse	mixed	mixed	mixed	mixed	direct
5	0.1	direct	inverse	mixed	mixed	direct	direct	direct
	10	direct	mixed	direct	direct	direct	direct	mixed

Table 6: Cascade type of the nonlinear transfers in the different regimes.

line $k = q$ (dashed line drawn in the figures), which corresponds to the exchange $(k \leftrightarrow q)$. Further clarifying the behavior of $T(\mathbf{k} \leftarrow \mathbf{q})$ is the surface of T as a function of k and q. The variation of the maximum values of the nonlinear transfer in the different regimes is given in Table 5. From Figs. 19 - 22, one can see that most of the activity of the nonlinear tranfer functions is close to the line $k = q$, which shows that the transfer occurs between scales of motion of similar scale, the transfer may be then properly described as a local cascade. When the positive contours lie above the $k = q$ line, there is an inverse cascade, towards large scales. A direct cascade, towards small scales, is specified when the positive contours are under the $k = q$ line. When the positive contours appear simultaneously above and under the $k = q$ line, without a clear dominant behavior, a mixed cascade is defined, with the transfer occurring simultaneously to both large and small scales. The cascade type for each of the nonlinear transfers is given in Table 6.

In all cases, the dominant nonlinear transfer is T^N (Figs. 19, 20 and Tables 5, 6).

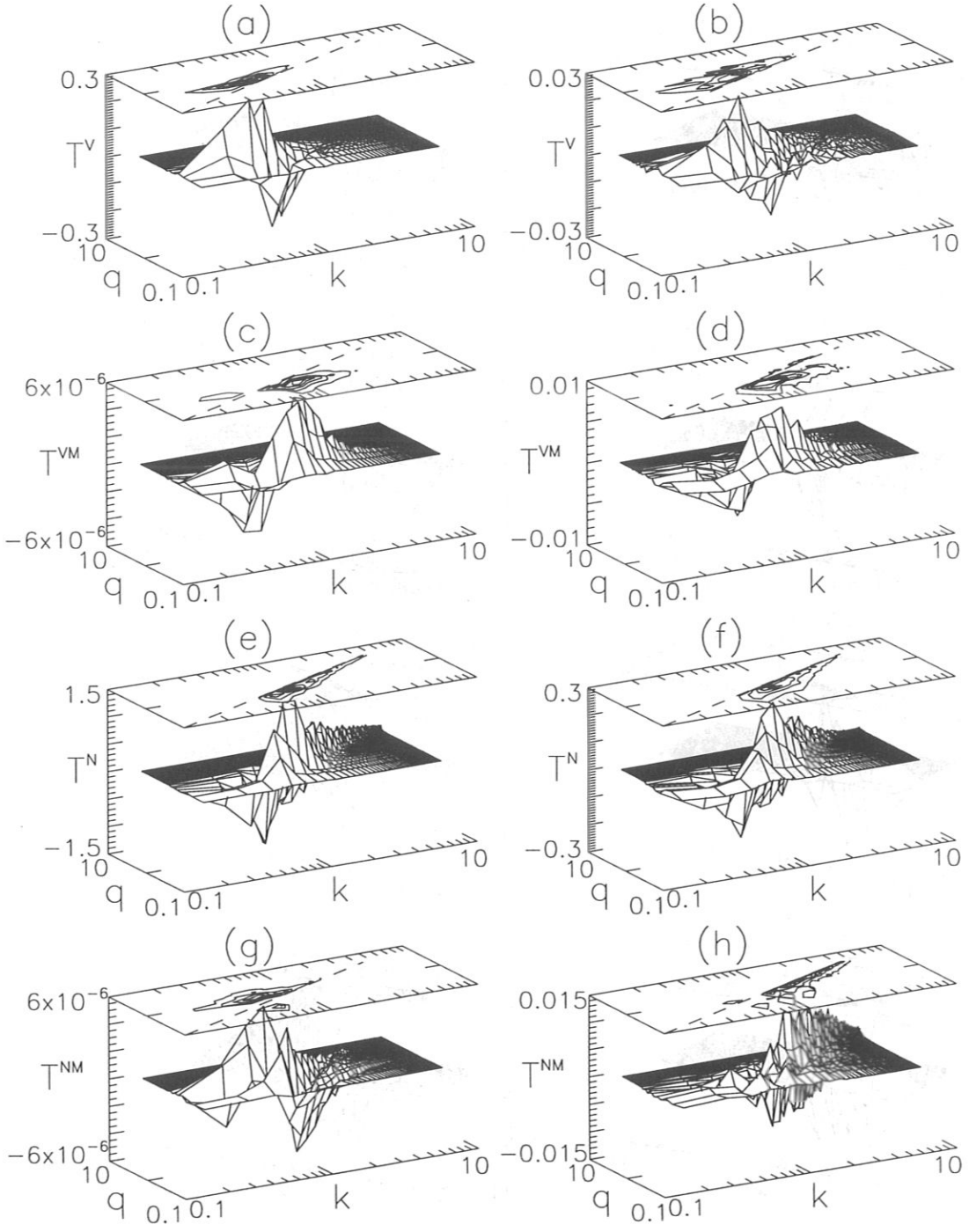

Figure 19: Nonlinear transfers of the energy components for $\mathcal{C} = 0.1$, $\beta = 0.001$ ((a), (c), (e) and (g)) and $\beta = 10$ ((b), (d), (f) and (h)).

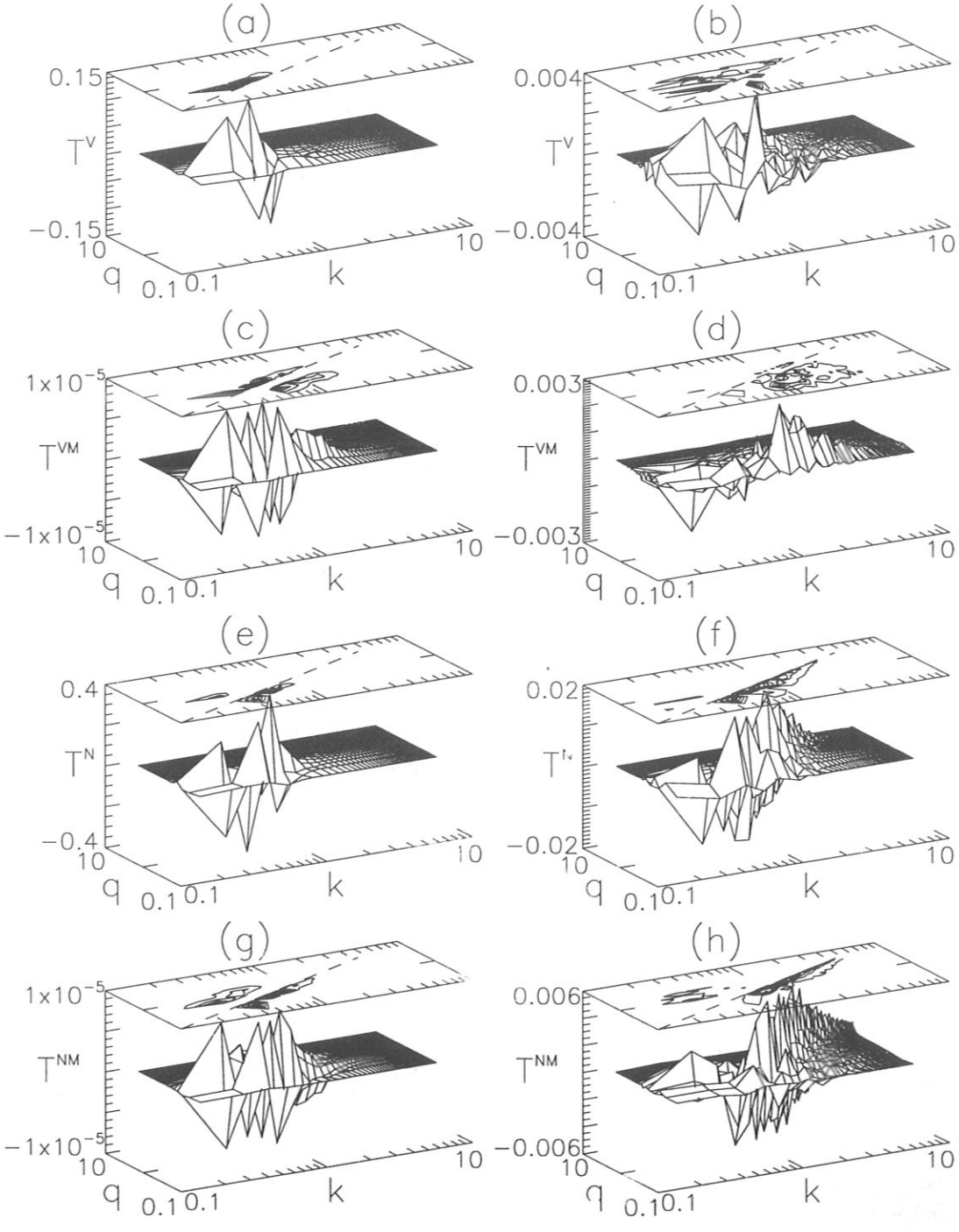

Figure 20: Nonlinear transfers of the energy components for $\mathcal{C} = 5$, $\beta = 0.001$ ((a), (c), (e) and (g)) and $\beta = 10$ ((b), (d), (f) and (h)).

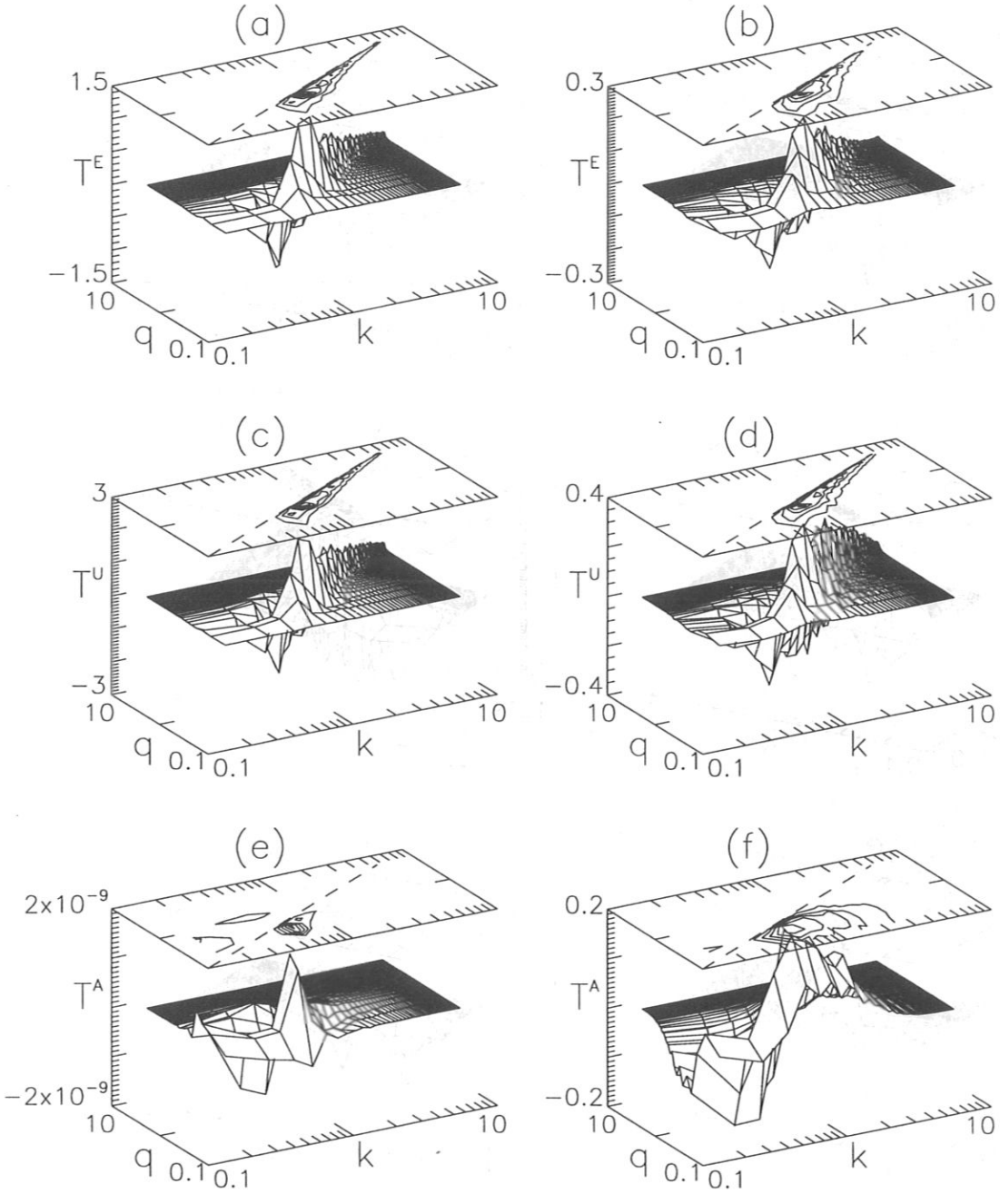

Figure 21: Nonlinear transfers of the invariants for $\mathcal{C} = 0.1$, $\beta = 0.001$ ((a), (c) and (e)) and $\beta = 10$ ((b), (d) and (f)).

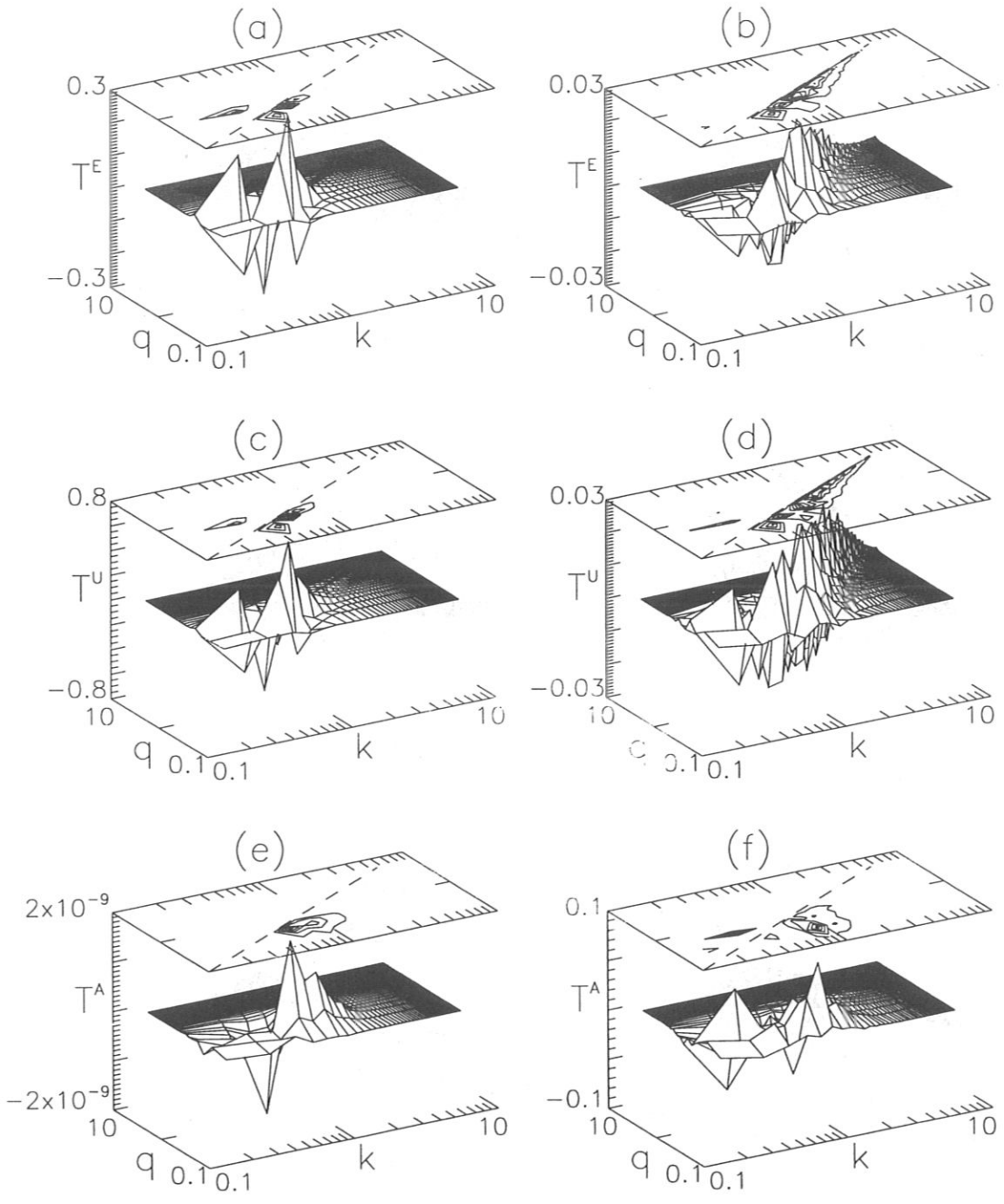

Figure 22: Nonlinear transfers of the invariants for $\mathcal{C} = 5$, $\beta = 0.001$ ((a), (c) and (e)) and $\beta = 10$ ((b), (d) and (f)).

Even in the electromagnetic regime, the terms responsible for the magnetic transfer of the energy, T^{NM} and T^{VM} are much smaller than T^N. T^N shows a direct cascade, as $\tilde{n}$ is passively advected by the $\mathbf{E} \times \mathbf{B}$ flow eddies. Even in the case $\mathcal{C} = 5$, which is the most sensitive to changes of β, T^N has always the same character, showing a direct cascade, with only the magnitude of T^N being sensitive to variations of β and $\mathcal{C}$. T^V shows an inverse cascade in the electrostatic limit. However, this character is modified when β is increased for $\mathcal{C} = 1$ and $\mathcal{C} = 5$ (mixed cascade), while the inverse cascade remain robust for $\mathcal{C} = 0.1$. The direct cascade contribution of T^V is already present in the electrostatic limit. Nevertheless, as the inverse cascade contribution is very strong, the direct cascade contribution cannot be seen in the contour plots. As β increases, the inverse contribution of T^V becomes weaker. Therefore, in the electromagnetic limit the direct contribution of T^V becomes more important and a mixed cascade appears (for $\mathcal{C} = 1$ and $\mathcal{C} = 5$). It is interesting to note that the dual cascade, which was observed for the Hasegawa-Wakatani system [34], with an inverse cascade of the electric potential and a direct cascade of the vorticity is still present in the electrostatic case. For increasing β, the vorticity continues to show a direct cascade. However, the electric potential sometimes presents a mixed cascade instead of the inverse cascade.

The nonlinear transfers involving the magnetic fluctuations $\tilde{\psi}$, T^{NM} and T^{VM}, are very small (negligible) in the electrostatic limit, as expected. In this limit, T^{NM} and T^{VM} have a mixed cascade character. As β increases, the direct cascade becomes stronger until in the electromagnetic limit, the direct cascade is clearly dominant for all values of $\mathcal{C}$ (Figs. 19, 20 and Tables 5, 6). By comparing the electrostatic limit with the electromagnetic limit, we can conclude that the magnetic fluctuations make the transfer of energy between the density and the potential fluctuations more difficult. Therefore, the response of the potential fluctuations $\tilde{\phi}$ to the density fluctuations tn is delayed, leading to the loss of adiabaticity in the electromagnetic limit. Hence, even though the nonlinear mixed transfer are still much smaller than T^N even for $\beta = 10$, their presence is enough to change the adiabaticity of the system. This enhancement of the nonadiabatic character is the most important contribution of the magnetic fluctuations energetic to the overall system.

Moreover, T^E, the resulting nonlinear energy transfer, is strongly dominated by T^N in all cases considered. For $\mathcal{C} = 0.1$, T^E shows a direct cascade independent of β (Fig. 21 and Table 6). In the adiabatic regime ($\mathcal{C} = 5$) for $\beta = 0.001$, T^E has a mixed cascade character, since in this limit T^V has an important role. As β increases this role diminishes and T^E shows the usual direct cascade (see Fig. 22 and Tables 6, 5). The nonlinear transfer of the enstrophy T^U shows a direct cascade, except in the case $\mathcal{C} = 5$ and $\beta = 0.001$. In this case the kinetic transfer has a more important role, changing the character of the transfer to a mixed cascade. However, even in this case the dominant behavior is the direct cascade. Therefore, the main effect of β on T^U is to change its magnitude, with the qualitative behavior of the nonlinear transfer being rather robust. T^A is the quantity that is most affected by β. Besides the expected increase of the magnitude of T^A, its qualitative behavior depends strongly on β and $\mathcal{C}$. For $\mathcal{C} = 0.1$ and $\beta = 0.001$, T^A presents a direct local cascade. When $\beta = 10$ the cascade is still direct, but involves a rather different range of modes, not so near the line $k = q$ (compare Fig. 21(e) and 21(f)). On the other hand, for

$\mathcal{C} = 5$, while the electrostatic limit is very similar to that of $\mathcal{C} = 0.1$, the electromagnetic limit has a mixed local cascade character.

In Fig. 23 we summarize the linear and nonlinear transfer of energy of the system. We chose as a typical example the case $\mathcal{C} = 0.1$ and $\beta = 10$. The arrows have thicknesses which are proportional to the logarithm of the quantities considered (multiplied by 10^3). On the left side, we show the linear transfer of a mode $k < k_m^E$ and on the right side of a typical mode $q > k_m^E$. These modes are then connected by the nonlinear transfers. The source of density energy Γ_n is present in both modes, but is stronger at k. The energy is then linearly transferred from $\tilde{n}$ to $\tilde{\psi}$ through Γ_n^p, while being dissipated in the smaller scales by D_N^E, D_M^E and Γ_r. Simultaneously the energy is being transferred nonlinearly from $\tilde{n}(k)$ to $\tilde{n}(q)$ in a direct cascade, represented by T^N (directed to smaller scales). The nonlinear transfers are represented by arrows in the direction of the cascade, however the sum of all the nonlinear transfers is zero. Besides the strong nonlinear transfer T^N the energy is also transferred nonlinearly from $\tilde{n}(k)$ to $\tilde{\psi}(q)$ (T^{NM}), which is also a direct cascade. The figure shows clearly how the presence of $\tilde{\psi}$ makes difficult to transfer energy from $\tilde{n}$ to $\tilde{\phi}$. In the small scales region ($q > k_m^E$), there is a weak linear transfer from $\tilde{\psi}$ to $\tilde{\phi}$ through Γ_V^p, but for the larger scales this linear transfer is in the opposite direction. $\tilde{\phi}$ is also related to $\tilde{\psi}$ through a direct cascade T^{VM}. Finally there is a strong nonlinear inverse cascade between $\tilde{\phi}(k)$ and $\tilde{\phi}(q)$ and a kinetic dissipation D_V^E (stronger at smaller scales). Fig. 23 shows clearly that the role of the magnetic fluctuation in the system is rather important for the energy transfer, even though the nonlinear transfers involving the magnetic fluctuations have a magnitude much smaller than the nonlinear transfers T^N and T^V. The magnetic fluctuations determine how strongly or weakly the density and potential fluctuations are related. It is important to notice that the energy transfer character is in agreement with the electrostatic studies [34, 50]. The magnetic fluctuations do not change the character of the nonlinear transfers T^N and T^V in the electrostatic system, only the linear transfer, which occurred between $\tilde{n}$ and $\tilde{\phi}$ is not present here in the same form. It bears repeating that the result of this transfer investigation has been to show that the most important effect of the magnetic fluctuations is to enhance the nonadiabatic character of the system by reducing the immediacy of the coupling between $\tilde{n}$ and $\tilde{\phi}$.

6 Conclusion

In this paper, we have presented detailed properties of the turbulent states of a simple drift-wave model with magnetic fluctuations. The system was solved numerically and compared with the known properties of its limiting cases, the 2-D Hasegawa-Wakatani and MHD equations.

The most important single conclusion is that although in certain limits the magnetic fluctuations have significant influence (near-adiabatic electrons, high β), the turbulence is largely electrostatic in character. This is particularly true with regard to the transport. We observed dominant magnetic influence only when β was as large as 10, a value quite far from the operational limits of current magnetic confinement devices ($\beta < 1$). In more

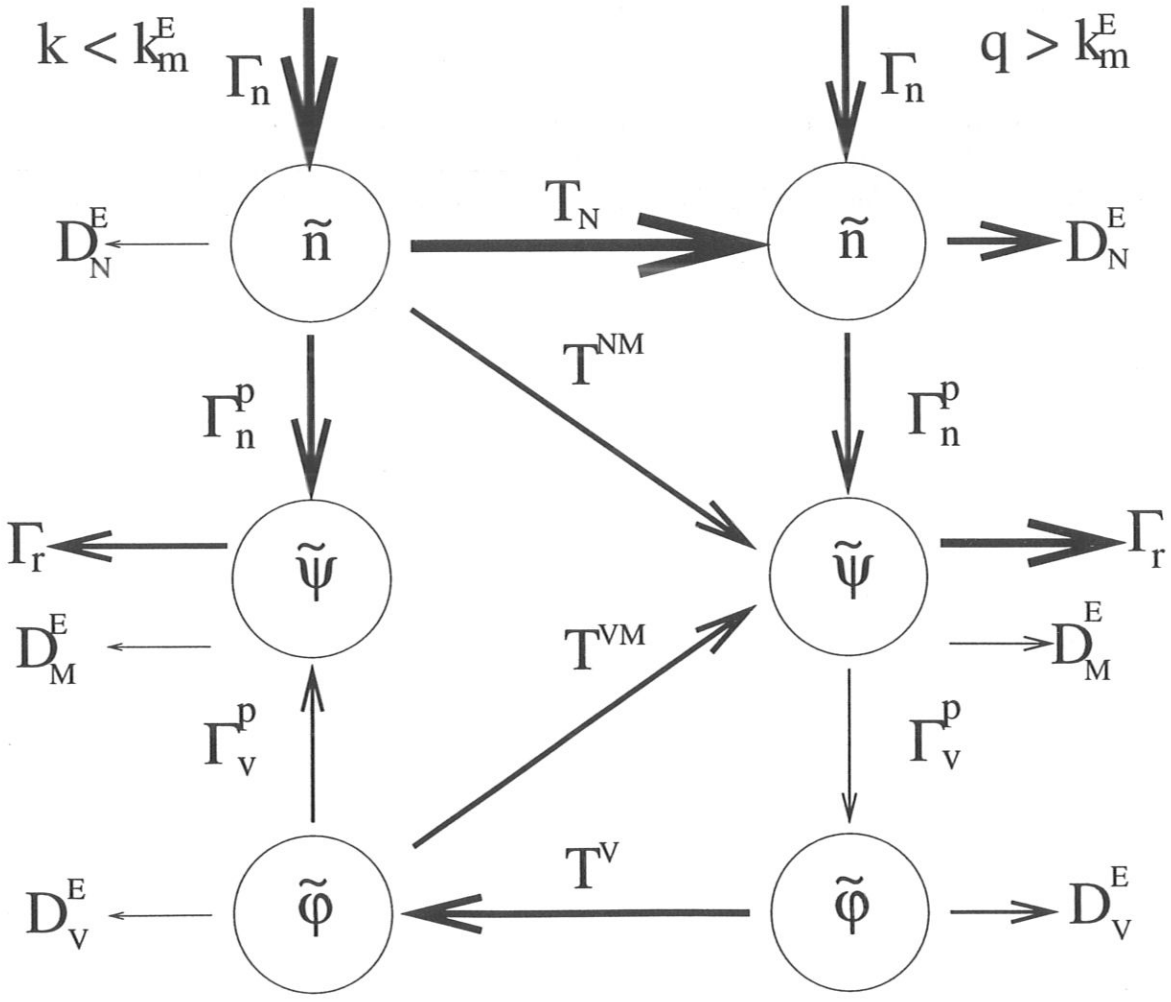

Figure 23: Nonlinear and linear energy transfers among the variables $\tilde{n}$, $\tilde{\phi}$ and $\tilde{\psi}$ for $C = 0.1$ and $\beta = 10$.

moderate situations, the magnetic part of the system was seen to be effective in enhancing the nonadiabatic character of the electron dynamics. In turbulence in a sheared magnetic field, the electron nonadiabaticity is already strongly enhanced, so that a preliminary study saw little effect of the magnetic fluctuations in the collisional regime [42]. However, the present results suggest that the hot plasma regime ($T > 1keV$) may be made less adiabatic than would be otherwise expected. Work is underway on a three-dimensional model which will test this directly in tokamak geometry.

In any case, the neglect of magnetic fluctuations should be done with extreme care, since as was seen in the energy transfer analysis, the magnetic part of the system has an important influence on the relation between density and electrostatic fluctuations, i.e., the nonadiabatic dynamics which determines the transport. Therefore, even if the turbulence can still be considered electrostatic, it is of importance to understand the role of the magnetic fluctuations in determining the characteristics of the turbulence in more realistic models.

References

[1] P. Liewer, *Nucl. Fusion* **25**, 543 (1985).

[2] A.J. Wootton, B.A. Carreras, H. Matsumoto, K. McGuire, W.A. Peebles, Ch.P. Ritz, P.W. Terry, and S.J. Zweben, *Phys. Fluids B* **2**, 2879 (1990).

[3] W. Horton, *Phys. Reports* **192**, 1 (1990).

[4] J.W. Connor, *Plasma Phys. Control. Fusion* **35** B293, (1993).

[5] K.H. Burrell, K.W. Gentle, N.C. Luthman, Jr., E.S. Marmar, M. Murakami, K.F. Schoenberg, W.M. Tang, and M.C. Zarnstorff, *Phys. Fluids B* **2**, 2905 (1990).

[6] A.H. Boozer, D.E. Baldwin, C.W. Horton, R.R. Dominguez, A.H. Glasser, J.A. Krommes, G.H. Neilson, K.-C. Shaing, W.L. Sadowski, and H. Weitzner, *Phys. Fluids B* **2**, 2870 (1990).

[7] H. Ji, H. Toyama, K. Miyamoto, S. Shinohara, and A. Fujisawa, *Phys. Rev. Lett.* **67**, 62 (1991).

[8] G. Fiksel, S.C. Prager, W. Shen, and M. Stoneking, *Phys. Rev. Lett.* **72**, 1028 (1994).

[9] G.X. Li, A. Möller, J.R. Drake, H. Bergsåker, J.H. Brzozowski, G. Hellblom, S. Mazur, P. Nordlund, and A. Welander, Proceedings of the *22nd European Physical Society Conference on Controlled Fusion and Plasma Physics*, Bournemouth, edited by B.E. Keen, P.E. Stott, and J. Winter (European Physical Society, Geneve, 1995), Vol. 19C, I, p. 173.

[10] A.J. Wootton, R. Bengtson, R.V. Bravenec, J. Chen, G. Cima, P.H. Edmonds, M. Freeman, H. Gasquet, K. Gentle, G. Hallock, Y. Karzhavin, S. McCool, D. Patterson, P. Phillips, B. Richards, D. Roberts, W. Rowan, D. Ross, E. Solano, D. Sing, R.F. Steimle, H. Tsui, J. Uglum, Y. Wen, Z. Zhang, R.F. Gandy, T.D. Rempel, M. Kwon, C. Watts, R. Durst, R.J. Fonck, D.L. Brower, Y. Jiang, W.A. Peebles, J.W. Heard, R.L. Hickock, A. Ouroua, P.M. Schoch, K.A. Connor, and G. Giruzzi, Proceedings of the *Fifteenth International Conference on Plasma Physics and Controlled Fusion Research*, Seville, 1994, IAEA-CN-60/A2/4-P-9 (1995).

[11] C. Hidalgo, *Plasma Phys. Control. Fusion* **37**, A53 (1995).

[12] J.W. Connor and H.R. Wilson, *Plasma Phys. Control. Fusion* **36**, 719 (1994)

[13] X. Garbet, F. Mourgues, and A. Samain, *Plasma Phys. Control. Fusion* **32**, 917 (1990).

[14] A. Hirose, A.I. Smolyakov, M. Elia, L. Zhang, and O. Ishihara, *Comm. Plasma Phys. Control. Fusion* **16**, 141 (1995).

[15] B.B. Kadomtsev and O.P. Potguse, in *Plasma Physics and Controlled Nuclear Fusion Research* (Proc. 7th Int. Conf. Vienna, 1978), IAEA, Vienna, Vol. 1, 649 (1979).

[16] F.A. Haas, A. Thyagaraja, and I. Cook, *Plasma Phys.* **23**, 1027 (1981).

[17] B.A. Carreras, P.H. Diamond, M. Murakami, J.L. Dunlap, J.D. Bell, H.R. Ricks, J.A. Holmes, E.A. Lazarus, V.K. Pare, P. Similon, C.E. Thomas, and R.M. Wieland, *Phys. Rev. Lett.* **50**, 503 (1983).

[18] M.A. Dubois, P. Ghendrih, B. Pégourié, R. Sabot, A. Samain, M. Zabiégo, and X.L. Zou, *Plasma Phys. Control. Fusion* **36**, B55 (1994).

[19] D. Biskamp, *Nonlinear Magnetohydrodynamics*, Cambridge University Press, Cambridge (1993).

[20] D. Montgomery, *Magnetohydrodynamic Turbulence*, in *Lecture Notes on Turbulence*, edited by J.R. Herring and J.C. McWilliams, World Scientific, Singapore, pp. 75-169, (1988).

[21] J.D. Callen, *Phys. Rev. Lett.* **39**, 1540 (1977).

[22] P.A. Duperrex, Ch. Hollenstein, B. Joye, R. Keller, J.B. Lister, F.B Marcus, J.M. Moret, A. Pochelon and W. Simm, *Phys. Lett. A* **106**, 133 (1984).

[23] K. Molvig, S.P. Hirshman, and J.C. Whitson, *Phys. Rev. Lett.* **43**, 582 (1979).

[24] R.E. Waltz, *Phys. Fluids* **28**, 577 (1985).

[25] E. Fernandez, P.W. Terry, and D.E. Newman, *Phys. Plasmas* **2**, 4204 (1995)

[26] A.A. Thoul, P.L. Similon, and R.N. Sudan, *Phys. Plasmas* **1**, 601 (1994).

[27] P.W. Terry, P.H. Diamond, and T.S. Hahm, *Phys. Rev. Lett* **57**, 1899 (1986).

[28] D. Pfirsch and D. Correa-Restrepo, IPP-Report 6/329 (1995). D. Pfirsch and D. Correa-Restrepo, to be published in *Plasma Phys. Contr. Fusion* (1996).

[29] B. Scott, Proceedings of the *22nd European Physical Society Conference on Controlled Fusion and Plasma Physics*, Bournemouth, edited by B.E. Keen, P.E. Stott, and J. Winter (European Physical Society, Geneve, 1995), Vol. 19C, **I**, p. 231.

[30] N. Mattor and P.H. Diamond, *Phys. Plasmas* **1**, 4002 (1994). N. Mattor, *Phys. Plasmas* **2**, 766 (1995).

[31] S. Raycharedhuri, *Nucl. Fusion* **35**, 1281 (1995).

[32] J.F. Drake, P.N. Guzdar, S. Novakovskii, C.S. Liu, A. Zeiler, and D. Biskamp, Proceedings of the *Fifteenth International Conference on Plasma Physics and Controlled Fusion Research*, Seville, 1994, IAEA-CN-60/D-P-I-8 (1995). A. Zeiler, D. Biskamp, J.F. Drake and P.N. Guzdar, IPP-Report 6/333 (1995).

[33] A. Hasegawa and M. Wakatani, *Phys. Rev. Lett.* **50**, 682 (1985).

[34] S.J. Camargo, D. Biskamp, and B.D. Scott, *Phys. Plasmas* **2**, 48 (1995).

[35] A.E. Koniges, J.A. Crotinger, and P.H. Diamond, *Phys. Fluids B* **4**, 2785 (1992).

[36] F.Y. Gang, B.D. Scott, and P.H. Diamond, *Phys. Fluids B* **1**, 1331 (1989).

[37] X.Q. Xu, R.H. Cohen, J.A. Crotinger, and A.I. Shestakov, *Phys. Plasmas* **2** (1995).

[38] D. Biskamp and A. Zeiler, *Phys. Rev. Lett.* **74**, 706 (1995).

[39] A. Hasegawa and M. Wakatani, *Phys. Fluids* **26**, 2770 (1983).

[40] R.D. Hazeltine, *Phys. Fluids* **26**, 3242 (1983).

[41] N. Bekki and Y. Kaneda, *Phys. Rev. Lett.* **57**, 2176 (1986).

[42] B. Scott, *Proceedings of the 21st EPS Conference on Controlled Fusion and Plasma Physics*, Montpellier, 1994, edited by E. Joffrin, P. Platz, and P.E. Stott (European Physical Society, Geneve, 1994), Vol. 18B, **II**, p. 560.

[43] B.D. Scott, *J. Comput. Phys.* **78**, 114 (1988).

[44] B.D. Scott, *Nucl. Fusion* **32**, 873 (1992).

[45] S.I. Braginskii, in *Reviews of Plasma Physics*, edited by M.A. Leontovich, (Consultants Bureau, New York, 1965), Vol. 1, p. 205.

[46] Ch. P. Ritz, E.J. Powers, and R.D. Bengtson, *Phys. Fluids B* **1**, 153 (1989).

[47] Y.C. Kim and E.J. Powers, *Phys. Fluids* **21**, 1452 (1978)

[48] B.Ph. van Milligen, C. Hidalgo, and E. Sánchez, *Phys. Rev. Lett.* **74**, 395 (1995).

[49] J.A. Domaradzski, *Phys. Fluids* **31**, 2747 (1988).

[50] B.D. Scott, *Phys. Fluids B* **4**, 2468 (1992).